INVESTIGATING THE STRUCTURE, SOLUBILITY AND BIOACTIVITY OF Na/Sr BIOACTIVE GLASSES/GLASS-CERAMICS

BY

YIMING LI

A THESIS

SUBMITTED TO THE FACULTY OF

ALFRED UNIVERSITY

IN PARTIAL FULFILLMENT OF THE REQUIREMENTS
FOR THE DEGREE OF

MASTER OF SCIENCE

IN

BIOMATERIALS ENGINEERING

ALFRED, NEW YORK

SEPTEMBER, 2014

INVESTIGATING THE STRUCTURE, SOLUBILITY AND BIOACTIVITY OF

Na/Sr BIOACTIVE GLASSES/GLASS-CERAMICS

BY

YIMING LI

B.S. CHONGQING UNIVERSITY OF TECHNOLOGY (2011)

SIGNATURE OF AUTHOR _____

APPROVED BY _____

ANTHONY W. WREN, ADVISOR

_____

NATHAN P. MELLOTT, ADVISORY COMMITTEE

_____

ALEXIS G. CLARE, ADVISORY COMMITTEE

_____

CHAIR, ORAL THESIS DEFENSE

ACCEPTED BY _____

DOREEN D. EDWARDS, DEAN

KAZUO INAMORI SCHOOL OF ENGINEERING

ACKNOWLEDGEMENTS

I would like to first and foremost, thank Dr. Wren for being a great advisor throughout my entire duration of my master studies and for the many opportunities and valuable pieces of advice he has given to me. I would also like to thank Dr. Hall, Dr. Misture and Dr. Mellot for their invaluable abilities as teachers. I've learnt much from them. In addition, I would like to thank Dr. Coughlan, Dimple Pradhan, Lana Placek, Yiyu Li, and Wirat Lerdpron for their great help on the experiments and writing of my master thesis. I could not do it without their help. I also want to thank my family and my friends. Thanks again everybody.

Published Work

- Y. Li, A. Coughlan, F.R. Laffir, D. Pradham, N.P. Mellott, A.W. Wren, "Investigating the Mechanical Durability of Bioactive Glasses as a Function of Structure, Solubility and Incubation Time," *Journal of Non-Crystal. Solids*, 380 25-34 (2013).
- Y. Li, A. Coughlan, A.W. Wren, "Investigating the Surface Reactivity of SiO_2–TiO_2–CaO–Na_2O/SrO Bioceramics as a Function of Structure and Incubation Time in Simulated Body Fluid," *Journal of Materials Science: Materials in Medicine*, 1-12 (2014).
- Y. Li, L.M. Placek, A. Coughlan, F.R. Laffir, D. Pradhan, N.P. Mellott, and A.W. Wren, "Investigating the Influence of Na^+ and Sr^{2+} on the Structure and Solubility of SiO_2-TiO_2-CaO-Na_2O/SrO Bioactive Glass," *Journal of Materials Science: Materials in Medicine* (Submitted, 2014).

Presented

- 39th Annual Northeast Bioengineering Conference (NEBEC), Syracuse, New York, April 5th -7th, 2013.
- Master's Level Graduate Research Conference, Brockport, New York, April 20th, 2013.
- 40th Annual Northeast Bioengineering Conference (NEBEC), Boston, MA, April 25th - 27th, 2014.

TABLE OF CONTENTS

Page

LIST OF TABLES

Page

LIST OF FIGURES

Page

ABSTRACT

This project was to investigate the structure, solubility and bioactivity of Na/Sr Bioactive glasses. There are three sections to this study. The first section is the effect of Na^+ and Sr^{2+} on the structure and biocompatibility of the glasses. Three glasses (*Ly-N, Ly-C, Ly-S*) were formulated with the substitution of sodium (Na^+) and strontium (Sr^{2+}) within the glass. X-ray diffraction (XRD), X-ray Fluorescence (XRF), Differential Thermal Analysis (DTA), Hot Stage Microscope (HSM) were used to characterize the series of glasses. Results of Network Connectivity (NC), X-ray Photoelectron Spectroscopy (XPS), Raman Spectroscopy, Magic Angle Spinning – Nuclear Magnetic Resonance (MAS-NMR) presented that the three glasses have very similar structure and Na^+ and Sr^{2+} both act as network modifiers. Cell Culture testing was conducted to investigate the biocompatibility and bioactivity of these glasses. The series of glasses have no negative influence on the cell viability, and addition of Sr^{2+} increase the cell viability. The second section investigates the mechanical durability of the bioactive glasses as a function of structure, solubility and incubation time. Samples were sintered to amorphous and crystalline structures. Ion release profiles were determined over 1, 7 and 30 days and in each case ion release was greatly reduced when the materials were crystallized. pH changes were reduced with the onset of crystallization compared to the amorphous counterparts. The highest concentrations of Na^+ (216 µg/mL) and Si^{4+} (172 µg/mL) both coming from *Ly-N* with amorphous structure. Crystalline samples presented much higher hardness values which did not reduce with respect to incubation time. However, the hardness of amorphous samples was found to experience significant reduction. The third part is simulated body fluid (SBF) testing and cytocompatibility of the glasses. In this section, sintered glass powder discs (amorphous /crystalline) were used to do SBF trials. Each material was subjected to maturation in SBF after 1, 7 and 30 days to describe any change in surface morphology. Scanning Electron microscopy (SEM) was used to observe the calcium phosphate (CaP) layers formed on the surface of each material. CaP deposition was observed predominantly on Na^+-containing amorphous and crystalline materials. Limited CaP deposition was observed on the surface of Sr^{2+}-containing crystalline materials. Cell culture analysis presented an increase in cell viability with Na^+-containing materials and a general reduction in cell viability with Sr^{2+}-containing material, however these reduction were not significant.

I. LITERATURE REVIEW

Artificial biomaterials are synthesized in the laboratory using a variety of chemical approaches utilizing metallic components, polymers, glasses, ceramics or composite materials. Bioactive glasses/glass-ceramics are often used for a medical applications. The first stage biomaterials were chosen to be as bio-inert as possible so that they minimize the formation of scar tissue. Then the field of biomaterials began to shift emphasis from a bio-inert tissue response to eliciting a controlled action and reaction in the physiological environment. The third-generation biomaterials combine resorbability and bioactivity with the aim of developing materials that help the body heal itself. [1] As a biomaterial, bioactive properties and functions of bioactive glasses/glass-ceramics used in orthopedics fields relate to their reactions with bone. Figure 1 shows the relationship between the compositions and bone-bonding bioactivity of SiO_2-Na_2O-CaO bioactive glass/glass-ceramic.

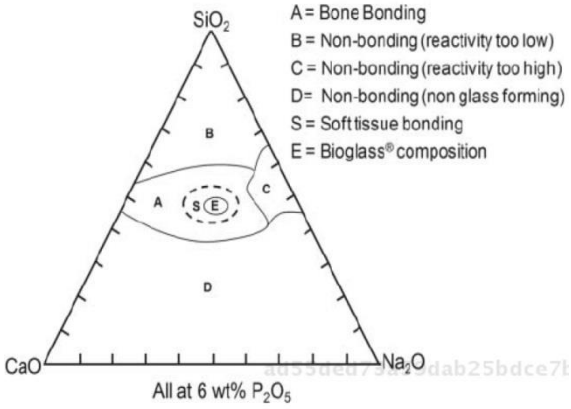

Figure 1. Bioactiveity maop of compositions in the SiO_2-Na_2O-CaO system (6wt% of P_2O_5) showing regions of bioactive response.[2]

Bioglass®, known as 45S5 bioactive glass, was the first material that was discovered to form a bond with bones. It was developed in the 1960s by Larry Hench after he tried to develop a material to fill bone voids without being rejected by body.[2] 45S5 Bioglass® compositions in weight percentage are: 45.0SiO_2-24.5Na_2O-24.5CaO-6.0P_2O_5 which has a silica based network with high concentration of network modifiers such as Ca and Na to degrade the glass network when immersed in fluids. As a biodegradable material, the glass degrades slowly in an aqueous

environment and these dissolution products can stimulate progenitor cells to differentiate into osteoblast cells. The procedure is called osteoinduction. The bioactive glass bonds to the existing bone and encourages new bone growth through the formation of calcium phosphate (or/and hydroxyapatite, HCA) layers on the glass surface which facilitates the osteogenesis mechanism. In order to take advantage of bioactive glasses in medical fields, research groups worldwide have developed novel bioactive glass compositions using the 45S5 composition as a guide. These bioactive glasses have been applied as bioactive coatings on the surface of metal implants, bioactive components of composites and have been made into synthetic bone scaffolds.

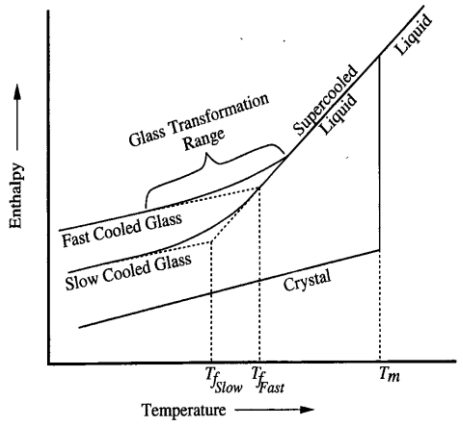

Figure 2. Effect of temperature on the enthalpy of a glass forming melt.[3]

A. Glass Formation

As a biomedical material, bioactive glasses can be designed containing different compositions to match different therapeutic requirements using numerous methods: the traditional melt-quench route, which was used in this project, sol-gel processing and chemical vapor deposition.[3] Different bioactive glasses still have two common characteristics as normal glass. They all have short-range periodic atomic arrangements and time-dependent glass transformation behavior. This behavior can be described basing on enthalpy versus temperature diagrams (Figure 2). In this process, an ideal small volume of liquid above the melting temperature is cooled with the atomic structure of the liquid changing gradually. The crystalline state, with the formation of long range periodic arrangements, occurs under any temperature below the melting point. The

viscosity increases with the decreasing of temperature and eventually keeps the atoms from rearranging to the equilibrium liquid structure. Then the viscosity of the liquid becomes fixed and no longer temperature-dependent. The temperature region lying between the limits where enthalpy is that of the equilibrium liquid and that of the frozen solid is the glass transformation region. The frozen solid is glass. The glass transformation region is a range of temperatures, but a certain set temperature was used to describe the onset of it. The certain temperature is termed the glass transformation temperature or the glass transition temperature (Figure 2). The glass transition temperature is an important characteristic of glass, and it can be used in cooperation with other characterization methods to estimate and analyze the structure and processing parameters of novel bioactive glasses.

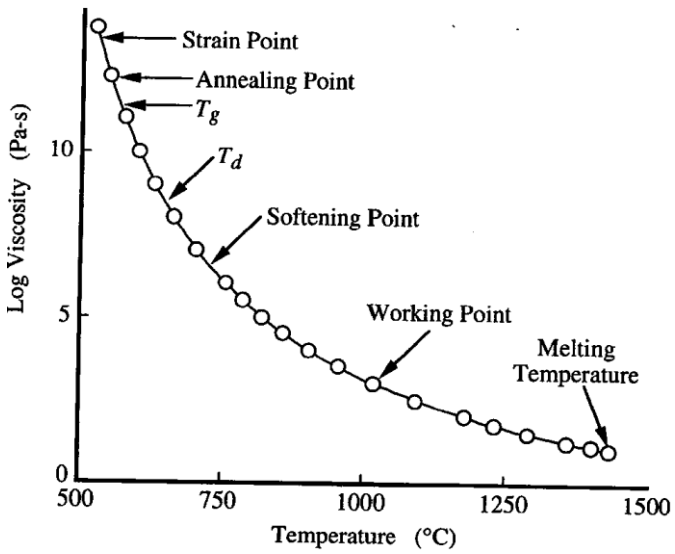

B. The Structure of Bioactive Glasses and Their Surfaces

The atomic structure affects all properties, in particular the bioactivity and degradation rate which directly influences the formation of HCA surface layer and cell viability. The structure of bioactive glasses can be described in the same way as other silicate glasses which have been well characterized in terms of the arrangement of the SiO_4 coordination tetrahedron (Figure 3(a)). The structure of pure SiO_2 consists of a three-dimensional network of SiO_4 tetrahedra, and each tetrahedron is associated with aa bridging oxygen in the structure (Figure 3(b)). The number of tetrahedron determines the size of ring (Figure 4(a)) used to characterize the network [4].

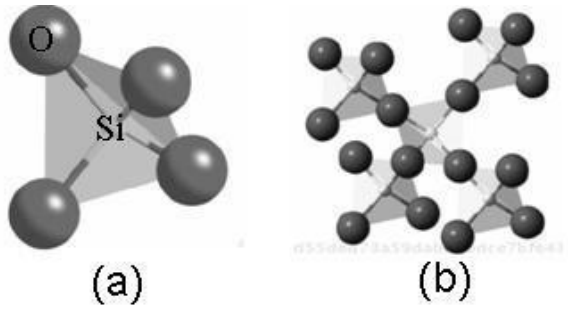

Figure 3. (a) A single SiO4 tetrahedron and (b) four tetrahedral linked to a central tetrahedron through bridging oxygen ions.[4]

When glass contains components, such as aluminum (Al) or alkali oxides, the network structure will be modified and disrupted **(**Figure 4). The oxygen atoms no longer fully bonded to two silicon atoms and are defined as non-bridging oxygen atoms (NBOs). For melt-derived bioactive glasses, such as Bioglass®, Na^+ and Ca^{2+} modify the structure of the glass inducing NBOs. The NBOs disrupt the links between nodes in the glass network leading to changes of the ring size. The NBOs depolymerize the tetrahedral network of the glass causing less interconnected glass network. Q_n can be used to characterize the distribution of NBOs over the tetrahedral structure units, where n refers to the number of bridging oxygen atoms surrounding the tetrahedron. Q_3 represents a tetrahedron with one non-bridging oxygen atoms (Figure 4(c)). [4] Another way to characterize structural modification is in terms of network connectivity (NC) which indicates the average number of bridging oxygen atoms on each tetrahedron. NC is an approximate quantity and it also has been found to be useful in predicting the tendency of glass

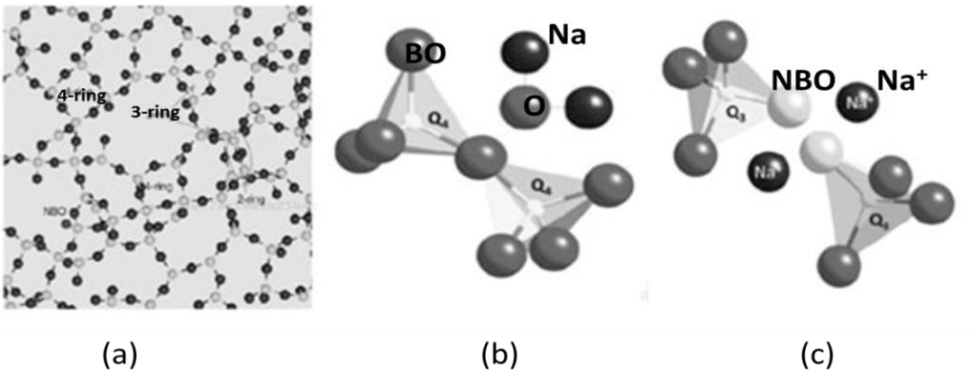

Figure 4. (a) Structure of simulated surface of vitrous silica. (b) Two Q_4 tetrahedral along with an Na_2O (c) The two tetrahedral are now both Q_3 Species.[4]

toward bioactivity. Glasses with NC greater than 2.4 are not likely to be bioactive. The rate of HCA layer formation and the percentage of new bone formation, *in vivo*, decrease rapidly when NC is greater than 2. In addition, glasses with NC>2 generally have higher energy barrier to overcome for crystallization than glasses with NC <2 owing to the stabilizing effect of cross-linking silicate chains [5]. Previous studies reported that NC affects HCA formation on SiO_2-CaO-Na_2O glass discs in simulated body fluid (SBF). Above NC of 2, the rate of HCA layer deposition decrease rapidly.[6]

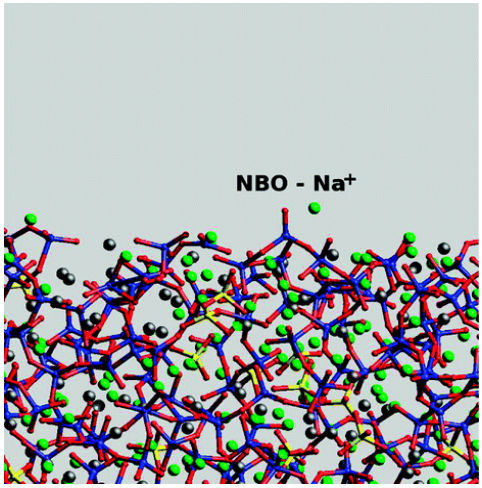

Figure 5. Side view of one of 45S5 relaxed surface.[7]

Tetrahedral network structure affects the activity and degradability of bioactive glasses it contains tetrahedral connected in smaller sized rings at the surface of glasses (Figure 5) where NBOs may be formed. These two-and three-membered rings, NBOs, and under-coordinated silicon will be the first to react with environmenta species, such as water. 2M rings are a common feature of the as-recreated bioactive glass surface. They are relatively stable against hydrolytic opening[2] making them potential adsorption and nucleation sites for calcium phosphate in the advanced stage of the bioactive bonding mechanism[7]. The ring structure (Figure 4(a)) is an identification of the glass network using Q_n units. M-fold rings denote cyclic silicates and M-membered rings for the residual cyclic structures (or local defects), where M = 2, 3, 4… represents the number of Qn units(or silicon atoms) which are presented in a ring[8].

As mentioned above, Na^+ is structural modifier for glass. The concentration of Na^+ on the surface of bioactive glasses is greater than their bulk structure and that of bio-inert glasses.[7] Rapid release of Na^+ from such layer proceeds by exchange with protons coming from the aqueous

contact solution. The Na^+/H^+ ion exchange results in increased local alkalinity and further hydrolysis (breaking of Si-O-Si bonds) of the glass network.[2] There is an association between the Na^+ and the surface NBOs to form $Na^+\cdots$NBO pairs that promote the dissociation of water through protonation of the NBOs. Some of them protrude out of the surface shown in Figure 5. The exposed Na^+ ions strongly attract water molecules and promote their initial penetration inside the surface. At the same time, they stabilize OH^- groups formed by water dissociation.[7]

The higher concentration of Na^+ ions, which combine the fragmentation of NBOs, promote network dissolution, leading to a more hydrophilic glass surface with release in solution of chainlike fragments and other silica species. This process directly impacts the bioactivity by nucleating the precipitation of calcium phosphate and activating key cellular processes. Therefore, the slower dissolution of glasses with more than 60mol% SiO_2 can be ascribed to their less hydrophilic nature due to higher silica and lower sodium contents. The domain way of Ca^{2+} release, another structural modifier, is Ca^{2+}-H_2O interactions.[9]

C. Bioactivity of Bioactive Glasses

In terms of bioactivity, bioactive glasses are able to bond with bone or/and stimulate new bone growth. There are two mechanisms of bioactivity associated with bioactive glasses. One is bone bonding to the HCA layer involving protein absorption, attachment of bone progenitor cells, cell differentiation and the deposition of bone extracellular matrix [1].

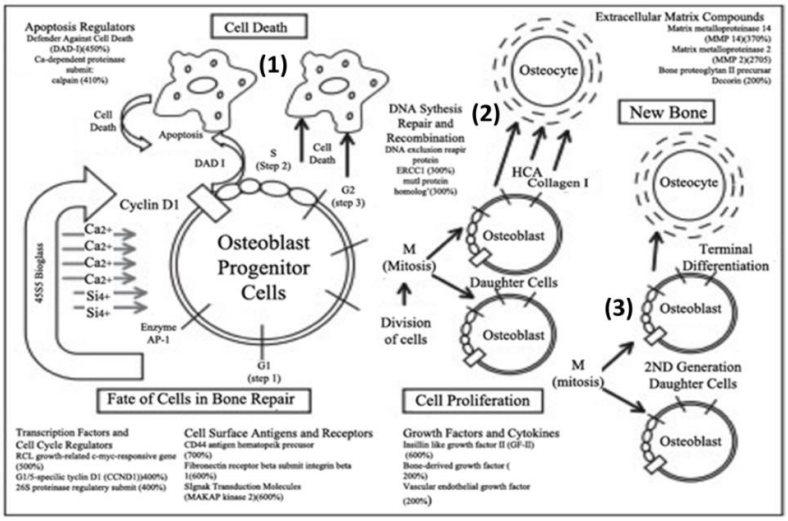

Figure 6. Schematic of Osteoblast progenitor cell cycle leading to (1) programmed cell death (apoptosis) (2) mitosis and cell proliferation, or (3) terminal cell differentiation toward an osteocyte.

Another mechanism is osteogenesis related to the action of dissolution products of the glasses on osteoprogenitor cells stimulating new bone growth. Figure 6 is the schematic of osteoblast progenitor cell cycle leading to (1) programed cell death (apoptosis) (2) mitosis and cell proliferation, or (3) terminal cell differentiation toward an osteocyte. (2) and (3) represent those two mechanisms of bioactivity.[10]

There are five stages for HCA formation in simulated body fluid (SBF) *in vitro* after accumulation of dissolution products inducing change of both the chemical composition and the pH of the solution to change: [11]

1. Rapid cation exchange of Na^+ and/or Ca^{2+} with H^+ from solution creates silanol bonds (Si-OH) on the glass surface: $Si - O - Na^+ + H^+ + OH^- \longrightarrow Si - OH^+ + Na^+(aq) + OH^-$ (Equation 1). The pH of the solution increases and a silica-rich region forms near the glass surface. Equation 1 describes the exchange process and the formation of HCA layer.
2. OH^- coming from high-pH solution attacks the silica glass network breaking Si-O-Si bonds. Soluble silica is lost in the form of $Si(OH)_4$ to the solution, leaving more Si-OH at the glass-solution interface: $Si - O \longrightarrow - Si + H_2O$ $Si - OH + OH - Si$ (Equation 1).
3. Condensation of Si-OH groups near the glass surface: repolymerization of the silica-rich layer.
4. The disassociative Ca^{2+} and PO_4^{3-} groups migrate toward the surface through the silica-rich layer from the solution, forming an amorphous $CaO-P_2O_5$ deposition on the silica-rich layer.
5. Incorporation of hydroxyls (OH^-) and carbonate from solution and crystallization of the $CaO-P_2O_5$ film to HCA.

After these 5 stages, the reaction layers enhance the adsorption and desorption of growth factors (stage 6) and decrease greatly the length of time that macrophages require to prepare the implant sites for tissue repair (stage 7). Osteoprogenitor cells colonize the surface of the bioactive

glass within 24-48h and start the production of various growth factors stimulating cell division, mitosis and the production of extracellular matrix proteins (stages 10) after attachment of stem cells (stage 8) and synchronized proliferation and differentiation of these cells (stage 9). Silica coming from $Si(OH)_4$ has been reported to stimulate collagen I production by osteoblast cells at a concentration of 10 mmol [12], and the highest gene expression observed at ~20µg/mL of soluble silica[13]. The next step is mineralization of the matrix and maturation of osteocytes in 6-12 days (stage 11). Figure 7 shows the 11 reaction stages occur at the surface of bioactive glasses leading to the bonding between the bone and the material.[10] Formation of HCA layer is a useful but not critical stage of reaction for bone generation. The other mechanism of bioactivity is osteoblast proliferation (daughter-second generation daughter transition) shown in the Figure 6 where growth factors and cytokines are necessary. Bioglass®45S5 can upregulate the concentration of unbound IGF-II representing the fraction of the molecule, IGFBP-3 (an IGF-II carrier protein), MMP-3 and Cathepsin-D (two proteases cleaving IGF-II from its carrier proteins) in an *in vitro* study.[14] IGF-II is a known inducer of osteoblast proliferation *in vitro*[15] and an anabolic peptide of the insulin family. In addition, it constitutes the most abundant growth factor in bone. The unbound IGF-II is likely to be responsible for the increase in cell proliferation observed.[16]

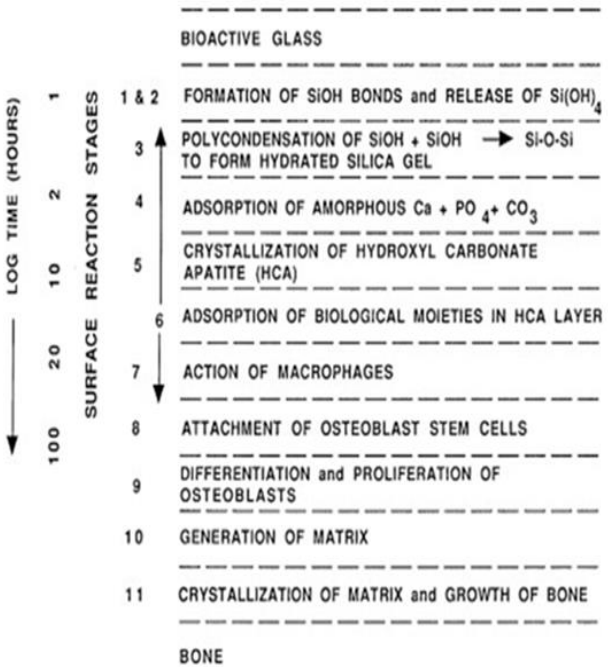

Figure 7. Sequence of interfacial reactions between bone and a bioactive glass or glass-ceramic.[10]

Based on these facts, bioactive glasses which cannot form HCA layers on the surfaces are still able to bond with bone and stimulate new bone growth. Therefore, cell culture testing is required for determining the biocompatibility of novel bioactive glasses.

D. Alternative Bioactive Glass Compositions

45S5 Bioglass® is the first generation bioactive glass and its composition has been a guide or starting point for research groups around the world to develop novel bioactive glasses investigating improved bioactivity and mechanical properties. Titanium (Ti^{4+}) and Strontium (Sr^{2+}), in this project, are relatively new additions, therefore the following section will explain why they were selected to be incorporated into the bioactive glass series utilized in this study.

1. Functions of Titanium in Bioactive Glasses

Ti is reported to increase the bioactivity of materials in numerous biomedical applications such as implantable devices in dental and orthopedic therapies as well as tissue engineering materials.[13] Some craniofacial/orthopedic implants were made from Ti-based materials due to their ability to facilitate close bone implant interfacial contact. In SBF trials, a calcium phosphate layer is deposited on the surfaces of Ti-containing materials including Ti_6Al_4V metal implants, Ti-N coated substrates and K_2O-SiO_2-TiO_2 glasses. The growth of the calcium phosphate layer could attribute to the modified surface where addition of Ti^{4+} leads to the formation of hydroxyl groups (Ti-OH) in the aqueous environment. Ti-OH structure promotes a negative charge, which favors surface precipitation of positive Ca^{2+} ions coming from solution.[7]

Previous studies on Ti-containing glasses determined Ti as a structural modifier.[17] Addition of Ti^{4+} made glasses more biodegradable by inducing more NBOs.[10] In terms of mechanical properties, a previous study revealed that the hardness values of bioactive synthetic bone scaffolds without Ti was lower than that of those containing Ti: 2.4 GPa (material without Ti), 7.1 GPa (material with 5 w% Ti) and 6.1 GPa (material with 10 w% Ti). Therefore, in this project, each glass contains 5 mol% (approxinately 5 wt%) TiO_2 in order to achieve good mechanical properties.

2. Function of Strontium in Bioactive Glasses

Strontium (Sr^{2+}) in human biology and pathology has attracted less attention than the other two important divalent cations Calcium (Ca^{2+}) and Magnesium (Mg^{2+}). However, Shorr and Carter[18] showed after giving a moderate dose of strontium lactate that the deposition of Ca^{2+} in bone was greater than total Ca^{2+} storage when Ca^{2+} was given without Sr^{2+}. There is increasing awareness of the biological role of Sr^{2+} after the development of the drug strontium ranelate. Strontium ranelate is a drug that acts as an effective antiosteoporotic therapy in treating osteoporosis. Unlike any other osteoporotic drugs, it has a dual effect on bone remodeling. Preclinical studies show that it results in increased bone mass, improving bone microarchitecture and strength in intact rodents. At the same time, it performed well in prevention of bone loss in osteopenic animals.[19] The research concerned with osteoporosis patients treated with strontium ranelate for 3 years revealed that the drug increased bone formation, which was assessed by both the mineralization rate and osteoblast concentration. Also, higher number of trabeculae, decreased trabecular separation, and an enhancement in cortical thickness was observed.[20]

In addition, Sr^{2+} is a bone-seeking trace element. At low dosage levels, stable Sr^{2+} was reported to improve vertebral bone density in osteoporotic patients and has beneficial effects on bone formation in rodents and humans.[21] The strontium levels in bone vary according to bone structure. Higher amounts of Sr^{2+} are found in cancellous bones than in cortical bone[22]. Furthermore, higher concentration of Sr^{2+} is observed in newly formed bones than in older bone. Sr also enhanced the replication of preosteoblastic cells, and stimulated bone formation in cell cultures *in vitro*.[23] The strontium-induced increase in bone formation results in better mechanical resistance of bone. In general, *in vitro*, Sr increases the number of osteoblasts and decrease the number and activity of osteoclasts.[24]

Sr^{2+} has a great affinity for bone as demonstrated by Sr incorporated into bones: surface exchange and ionic substitution. Surface exchange is an initial rapid mode absorption method depending on osteoblastic activity. During this procedure, Sr^{2+} is taken up by ionic exchange with bone Ca^{2+} and binding of Sr^{2+} to preosteoid proteins subsequently occurs. Ionic substitute is a second slower mechanism involving the incorporation of Sr^{2+} into the crystal lattice of the bone mineral.[24]

According to aforementioned facts, Sr^{2+} was incorporated into these bioactive glasses. Studies by Donnell *et a.l* produced a series of ten glasses based on 45S5 Bioglass®, where 0% to

100% of the calcium was substituted with strontium on a molar basis. The distribution of glass network former and modifier did not change across the series. This study presented that Sr^{2+} could be added to bioactive glasses to replace or combine with Ca^{2+} with little influence on glass physical properties. These strontium-substituted bioactive glasses will be useful for a range of applications in orthopaedic regenerative medicine. Calcium phosphate formed in SBF trials after 1 week or less. [23] A study on a series of zinc-calcium-strontium-silicate glasses and an additional study on strontium-containing phosphate glasses both presented good biocompatibility.[25] Furthermore, Gorustovich *et al.* evaluated the osteoconductivity of strontium-doped bioactive glass particles implanted in rat tibia bone marrow. The results revealed that these glass particles are osteoconductive when implanted inside the intramedullary canal of rat tibiae.[21]

E. Applications of Bioactive Glasses

1. Bioactive Glass Coatings

Bioactive glasses have been studied and used in medical applications including small-bone substitutions, controlled drug delivery systems, bone cements, and generally non-loading-bearing applications.[26] However, poor mechanical properties in tension or under cyclic loading limit the applicability of bioactive glasses. Metallic materials are better choices when mechanical properties are taken into account. Metallic alloys (Titanium (Ti) alloys, Cobalt (Co)-Chromium (Cr) alloys), Aluminum (Al) and Zirconium (Zr) are widely used in orthopedic field. However, problems still remain due to their poor bioactive and biocompatible capabilities. According to previous studies, bioactive glass or glass-ceramic coatings provide a resolution giving several interesting advantages: (1) they avoid corrosion and degradation of the substrate, (2) they protect the surrounding tissues from adverse interactions with debris coming from the substrate, (3) they promote the bioactive fixation of the implant to the living bone inducing osteointeragtion[27], (4) they can be easily modified to deliver ions such as antibacterial silver[28]. Some applications will be introduced in the following section.

Ti alloys and Co-Cr alloys used in the fabrication of prosthetic implants are very reactive. The reactions at the interface of glass/metal promotes the adhesion and bioactivity when they were coated with a SiO_2-Na_2O-K_2O-CaO-MgO-P_2O_5 glass.[29] Especially, the firing temperature should

be below the α - β phase transformation of Ti, between 885°C and 950°C for unalloyed Ti, depending on the impurity content, and between 955°C and 1010°C for Ti_6Al_4V to avoid degradation of the mechanical properties of the implant. Another matter that needs attention is the thermal expansion coefficients of the bioactive glasses are typically much larger than those of Ti alloys.[29] Increasing the Si content is a simple way to reduce the thermal expansion, but it is at the cost of bioactivity. Co-Cr alloys can be coated by the bioactive glasses with lower Si content.[29]

It has been reported that silica content below 60 wt% and the partial substitutions of CaO by MgO and Na_2O by K_2O are necessary for glass coatings on Ti-based metallic substrates to match the thermal expansion coefficients without cracking or delamination.[29] The optimum adhesion occurred when the interfacial layers with 100-200 nm thickness formed. In a study about bioactive glass coatings for orthopedic metallic implants made of Ti-based and Co-Cr alloys, an interfacial Ti_5Si_3 layer or continuous CrOx layer formed between the substrate and the coating indicating that they bond together chemically. The main reactions between the glass and the alloy are: $8Ti+3SiO_2 \rightarrow Ti_5Si_3+TiO_2$; $Cr + 3/2\ Na_2O \rightarrow 1/2\ Cr_2O_3 + 3Na$. In addition, the excessive reaction must be prevented, because it will lead to the loss of adhesion through the formation of a thick reaction layer accompanied by bubbles in the glass.[29] These results have been used on commercial dental implants.

Besides, bioactive glass-matrix/Ti particle composite coatings have been deposited on Ti-based alloy substrates using vacuum plasma spraying (VPS) technique. VPS has higher deposited speed, better control of the substrate degradation and the morphology and properties of the coatings compared to the traditional enameling method.[30]

Aluminum (Al) is a reliable material for orthopedic surgeries due to high wear resistance and fracture toughness. At the same time, it is an almost inert material without forming any chemical bonding with bone, which arouses loosening and clinical failure.[31] Alumina-based metallic materials have been coated by bioactive glass-ceramics to combine the mechanical properties of the substrate with the bioactivity of the coatings. The main difficulties in coating Al-based substrates are connected with its low thermal expansion coefficient and its high reactivity with glasses and glass-ceramics at high temperatures involving in the coating preparation.[31] Previous studies reported that at high temperature Al^{3+} extensively diffuses from the substrate to the coating surface contaminating the coating and negatively influencing its bioactivity.[32]

As a result, double-layer coatings on alumina substrate were developed to solve the problem. For instance, an intermediate SiO_2-CaO-based glass (SC) layer was interposed between alumina substrate and the glass-ceramic (SiO_2-Al_2O_3-P_2O_5-K_2O-CaO-F) layer (SAF). SAF is so viscous that it cannot effectively adhere to alumina substrates. Therefore, SC layer was expected to increase adhesion between the coating and the substrate. Furthermore, the similar thermal expansion coefficients of SC and SAF effectively avoid cracking because of residual thermal stresses. SC layer presented a very good adhesion to the alumina substrate without residual porosity. A continuous interface also formed between SAF and SC[31]. Good cell adhesion of coated samples indicated no Al^{3+} diffusion from the substrate. Better bioactivity of coated material was confirmed by four-day proliferation: the number of osteoblast-like cells on the surface of coated material was significantly higher than that of original alumina substrate.[31]

Zirconia bioceramics possess attractive mechanical properties that have been widely used in densitry and orthopaedics.[33] Yttria stabilized tetragonal zirconia (YSTZ, 94.5% ZrO_2 + 5.5% Y_2O_3) is stiff, wear resistant and chemically inert.[34] In current studies, YSTZ performed better when implanted in the healthy bones of rats than other materials.[33] However, a significant decrease in the affinity index was obtained with ovariectomy-induced osteopenia.[34] Affinity index was defined as the length of bone contact/the total length of the bone–implant interface×100%.[35] In order to reduce the adverse influence, YSTZ coated by RKKP® [36] (43.82 SiO_2, 24.23 β-$Ca_3(PO_4)_2$, 18.40 CaO, 4.55 Na_2O, 0.19 K_2O, 2.79 MgO, 4.94 CaF_2, 0.99 Ta_2O_5, 0.09 La_2O_3 (wt%)) presented good biocompatibility and osteogenic properties when used in studies involving healthy bones of rats.[37]

The bioactive glass RKKP® was applied as an enamel to the surface of the YSTZ samples with further sintering.[38] After being implanted and surrounded by cancellous bone, SEM and EDS images of the uncoated samples depicted a low degree of bone-prosthesis contact. On the contrary, good contact at the material-bone interface formed for the coated materials, and the bone surrounding the implant showed regular trabecular architecture revealing good osteointegration.[37]

2. Bioactive Glasses as Synthetic Bone Scaffolds for Tissue Engineering

In the last 20 years, tissue engineering has been considered as a promising approach for the repair and regeneration of tissue, damaged as a result of traumatic injuries, disease, or aging. Such situation for bone is outstanding: an estimated 2.2 million bone graft procedures are performed

annually to promote fracture healing, filling defects or repair spinal lesions worldwide.[39] Autograft is the best choice for treating bone defects, while limited supply and donor site mobility are problematic. Allograft is an alternative to autograft. Unfortunately, it is expensive and possibly lead to disease transmission and adverse host immune responses. The metal grafts, such as Ti_6Al_4V and Co-Cr, can provide mechanical support for bone replacement or fracture repair in loading-bearing situation, however they cannot self-repair like natural bones and become loose after implantation due to promoting bone resorption. Table I shows the standard ideal synthetic bone scaffold.

Table I. Requirements for Synthetic Bone Graft[42]

1. ***Biocompatible and Bioactive,*** promoting bone formation , and bond to the bone without soft tissue encapsulation
2. ***High porosity*** with an interconnected pore network to facilitate migration of cells, enabling fluid flow for nutrient supply and the removal of cellular waste products and to permit vascular invasion.
3. ***Suitable bioactivity*** to exploit the body's natural repair process, with biological response similar to that achieved by bioactive glasses
4. ***Biodegradable*** with predictable and safely biodegradation rate matched to the formation rate of neo-tissue
5. Sufficient mechanical competence
6. ***Easy to be produced and shaped*** to fit a range of defect geometries and up-scalable for mass production

Synthetic bone scaffolds made of bioactive glasses aroused researchers' interests as a new bone substitutes. Besides having excellent bioactive and biocompatible capabilities, bioactive glasses can be manufactured into porous 3D structure facilitating cell-proliferation and formation of new bone. In addition, the rate of degradation can be controlled by tailoring the structure and chemistry of the glasses to match that of bone ingrowth and remodeling.[39] 45S5 Bioglass®[40], a silicate bioactive glass designed 13-93[35,36], a borate bioactive glass designed 13-93B3[41] and bioactive glass 6P53B have been reported to be manufactured into a 3D synthetic bone scaffolds and presented good bioactivity.

However, limiting factors still exist when apply bioactive glass scaffolds for repair of defects in load-bearing bones: low strength and brittleness. The compressive strength of 45S5 Bioglass® scaffolds made by polymer foam replication technique (about 0.5 MPa) is much lower than that of human bones (Table II.). The relative low compressive strength comes from sintering, which is prone to crystallization at sintering temperatures above 1000°C.[43] Crystallization decreased the tendency of the glass to densify by viscous flow sintering. As a result, voids remaining from the burnout of the polymer foam are difficult to fill and remain as triangular-shaped pores in the struts leading to reduction of the strength. Nonetheless, current studies show that the bioactive glass scaffolds can be manufactured with both porous structure and strength comparable to human cancellous and cortical bone by optimizing composition, processing and sintering conditions. The compressive strength of 13-93 bioactive glass scaffolds with 85±2% porosity and 100-500μm pore size prepared by a polymer foam replication technique is 11±1 MPa. It is comparable with that of human cancellous bone.[44] The compressive strength of bone scaffolds made from bioactive 6P53B glass with 60% porosity is 136 MPa comparable with cortical bone. Therefore, to some extent, compositions of bioactive glasses influence the mechanical properties of the synthetic scaffolds made of bioactive glasses.

Table II. Summary of the Mechanical Properties of Human Bone[42]

	Compressive Strength (MPa)	**Flexural Strength (MPa)**	**Tensile strength (MPa)**	**Modulus (GPa)**	**Fracture toughness ($MPa \cdot m^{1/2}$)**	**Porosity (%)**
Cortical bone	100-150	135-193	50-151	10-20	2-12	5-10
Cancellous bone	2-2	10-20	1-5	0.1-5	0.1-0.8	50-90

Excluding composition and processing, sintering conditions largely influence the mechanical properties of scaffolds. It has been reported that the compressive strength of 45S5 Bioglass® scaffolds changed along with different processing and sintering temperatures**.** In terms of 13-93 bioactive glass scaffolds, the mechanical properties of the scaffolds produced by robocasting technique (compressive strength of 86±9 MPa, elastic modulus of 13±2 GPa and a Weibull modulus, an index for reliability, of 11±3 MPa[45]) are much better than those of the scaffolds made by polymer foam replication technique. The robocasting, a technique that

combines an extrusion process with a computer-guided positioning system by extruding a continuous filament, can be used to build 3D structure layer by layer.[46]

Mechanical stability of scaffolds in SBF and *in vivo* trials is another factor to be considered. The mechanical properties of scaffolds decreased rapidly because of biodegradation. The strength of 13-93 bioactive glass scaffolds produced by robocasting technique decreased from 86±9 MPa to 58±5 MPa in SBF and 35±4 MPa *in vivo* after 2 weeks, to 52±10 MPa in SBF and 16±4 MPa *in vivo* after 12 weeks. The elastic modulus decreased from 13±2 GPa to 9±2 GPa and 2±1 GPa respectively after 12 weeks in SBF and *in vivo*.[45] These facts reflected that achieving good bioactivity without sacrificing mechanical properties is still the limit for the application of bioactive glass synthetic bone scaffolds.

3. Composites Containing Bioactive Glasses

Another application of bioactive glasses is acting as composites combined with polymers, another prevalent material for synthetic bone repair, especially biodegradable synthetic polymers such as poly lactic acid (PLA), high molecular weight poly (L-lactic) acid (PLLA), poly (DL-lactic) acid (PDLLA) and poly (glycolic acid) (PGA). Bioactive glass additions improve the bioactivity of polymer scaffolds and control their degradation rate.

Synthetic bone scaffolds can't completely replace natural bones due to bone's complicated hierarchical structure[45]. Bones are composed of an organic (collagen (polymer)) phase and an inorganic (bone mineral (ceramic)) phase. Collagen, as a natural polymer with high tensile and flexural strength, provides a framework for the bone structure. Synthetic polymers are commonly used to make bone scaffolds because of the similar structure with collagen.[45] In addition, compared to natural polymer, synthetic degradable polymers can be produced under controlled conditions getting general predictable and reproducible mechanical and physical properties such as tensile strength, elastic modulus and degradable rate. Unfortunately, these polymer scaffolds would fail prematurely due to bulk erosion.[43] After implantation, water will be absorbed into the polymer cleaving chains leaving carboxylic acid (-COOH) groups. The chain-scission reaction will be accelerated when the pH decreases from neutral level. Therefore, the acidic groups increase the degradation rate. More and more short chains migrating from the material leads to reduced mechanical properties. In addition, the rapid release of acidic products under degradation causes serious inflammatory response.[43]

Another important driving force behind the development of polymer/bioactive glass composite scaffolds for bone engineering is remedying limitations mentioned above. It has been reported that addition of bioactive phases (glasses/ceramics) altered the polymer degradation behavior inducing rapid exchange of protons in water for alkali cations. These alkaline releasing products function as pH buffer at the polymer surface modifying the acidic polymer degradation. Inclusion of 45S5 Bioglass® has been proved to increase water adsorption compared to pure polymer foams of PDLLA.[47] Ideally, the degradation and resorption kinetics of composite scaffolds are designed for cell proliferation and growth of new cells and tissues. Previous study indicated that PDLLA/Bioglass® foam scaffolds provided an appropriate microenvironment for bovine annulus fibrous (BAF) cell culture enhancing cell proliferation and promoted the production of collagen type I and II compared to the pure PDLLA scaffolds. This fact provided preliminary evidence for use of this composite scaffolds as cell-carrier materials.[48]

Glass or ceramic fibers can also be dispersed in the polymer matrix to reinforce polymers and increase their stiffness.[45] The modulus of PLLA, PDLLA and PLGA composits with Bioglass® were much higher than that of pure polymers. The volume fragment of bioactive glass influenced the porosity of the composite scaffolds. It has been reported that the addition of bioactive glass (BG) from $3CaO\text{-}P_2O_5\text{-}MgO\text{-}SiO_2$ system was capable to tailor the porous structure of PLLA scaffolds prepared by thermally induced phase separation (TIPS) technique. BG particles acted as nucleating agents for PLLA crystallization, and the glass solubility controlled the pore size. The addition of BG promoted pore enlargement due to ions (Ca^{2+}, Mg^{2+}) leaching from the BG surface which increased the surface tension of water-rich phase and the interfacial tension between the polymer-rich phase and the polymer-poor phase. A significant increase in the pore size distribution was observed in the polymer scaffolds with the incorporation of bioactive glasses. However, the composite scaffolds with higher bioactive glasses content had poorer mechanical properties such as elastic moduli and compression strength.[49]

Based on the literature review, bioactive glasses/glass-ceramics have excellent bioactive and biocompatible capabilities. Na^+ and Sr^{2+} have previously been reported to promote the bioactivities of bioactive glasses/glass-ceramics, therefore, in this study, three glasses (*Ly-N, Ly-C, Ly-S*) were formulated by modifying the concentration of Na^+ and Sr^{2+} within the glass to investigate any change in the structure, solubility and bioactivity of a $SiO_2\text{-}TiO_2\text{-}CaO\text{-}Na_2O/SrO$ glass series.

II. MATERIALS AND METHODS

A. Glass Sample Preparation

Three glasses (***Ly-N, Ly-C, Ly-S***) were formulated to investigate any property changes with the substitution of sodium (Na^+) and strontium (Sr^{2+}) within the glass. The control group was formulated with equal quantities of Na^+ and Sr^{2+}. The compositions of the glasses are presented in Table 3. Glasses were prepared by weighing out appropriate amounts of analytical grade reagents (Fisher Scientific, Pittsburg PA, USA) and ball milling (1 h).

Table III. The Compositions of the Glasses (mol.fr)

	SiO_2	TiO_2	CaO	Na_2O	SrO
Ly-N	0.55	0.05	0.22	0.18	0.00
Ly-C	0.55	0.05	0.22	0.09	0.09
Ly-S	0.55	0.05	0.22	0.00	0.18

1. Glass Powder Preparation

The powdered mixes were oven dried (100ºC, 1 h) and fired (1,500ºC, 1 h) in a platinum crucible and the glass frit was shock quenched in water. The resulting frits were dried, ground and sieved to retrieve glass powders with a particle size less than 25 μm.

2. Glass Rods Preparation

Glass rods used for X-ray Photoelectron Spectroscopy (XPS) were produced in the following procedures. The powdered mixes were oven dried (100ºC, 1 h) and fired (1500ºC, 1 h) in platinum crucibles. Glass castings were produced by pouring the glass melts into graphite molds which were preheated to Tg. The graphite molds were left for 3 h and furnace cooled in order to anneal the glass. A diamond bladed, on an Isomet 5000 Linear Precision Saw (1500 rpm, 0.4 mm/min), was used to cut the resulting glass. Then they were shaped into Rods of (15×3ϕmm) using a Phoenix 4000 grinding machine with 60μm silicon carbide grinding paper, Buehler, IL, USA (High resolution XPS).

3. Glass Plates Preparation

Glass plates were made for XRF. The powdered mixes were oven dried (100ºC, 1 h) and fired (1500ºC, 1 h) in platinum crucibles. Glass plates measuring >18mm in diameter were produced by pouring molten glass on a graphite plate that was pre-heated to the samples Tg. The glass plates were then annealed for 3 h and furnace cooled.

4. Glass Buttons Preparation

Glass buttons (6 for each glass) were produced for cell culture testing. The powdered mixes were oven dried (100ºC, 1 h) and fired (1500ºC, 1 h) in platinum crucibles. Glass buttons were produced by drilling holes (8mm) in a flat graphite plate measuring 4mm in thickness. This mold was placed on another flat graphite plate and heated to the individual samples T_g. Molten glass was poured into each button mold and pressed to form an approximately uniform 4 x 8ϕ mm button. Each button was annealed for 3 h and furnace cooled, and then ground and polished using 60µm silicon carbide grinding paper (Buehler, IL, USA). Final glass buttons were polished further to fine and transparent in 2x 8ϕ mm, then ultrasonically cleaned and autoclaved.

5. Glass Powder Discs Preparation

Glass discs were produced by pressing glass powder into discs (1.5x8ϕ mm, n=3) and annealed/sintered to amorphous or crystalline structure according to the results of Differential Thermal Analysis (DTA) and Hot Stage Microscope (HSM). These samples were used for simulated body fluid (SBF) testing and ion release profiles, cell culture and hardness testing.

B. Effect of Na^+ and Sr^{2+} on the Structure and Biocompatibility of the Glasses.

1. Glass Characterization

1.1 X-ray Diffraction (XRD)

Diffraction patterns were collected using a Siemens D5000 XRD Unit (Bruker AXS Inc., WI, USA). Glass powder samples were packed into standard stainless steel sample holders. The glass discs were packed into the plastic sample holders. A generator voltage of 40 kV and a tube current of 30 mA was employed. Diffractograms were collected in the range $10°<2\theta<80°$, at a scan step size 0.02° and a step time of 10s. Any crystalline phases present were identified using JCPDS (Joint Committee for Powder DiffractionStudies) standard diffraction patterns.

1.2 X-ray Fluorescence (XRF)

The compositions of the glasses were calculated by X-ray fluorescence using the S4 Pioneer (Bruker AXS Inc, MA, USA). Glass plates (>18mm in diameter) were placed in a holder with an 18mm mask (thus revealing 18mm diameter of the glass for testing) and underwent testing using the Multi_Vac 18 program. The results were quantified using the Spectra Plus Launcher (Bruker) and normalized to 100.

1.3 Network Connectivity (NC)

The network connectivity (NC), the average number of bridging oxygens per [SiO_4] tetrahedron, was calculated by Equation 2. Where BO is the total number of bridging oxygens per network-forming ion, NBO is the total number of non-bridging oxygens per network modifier ion. NC calculations were performed assuming that Ti performs as a network former and also as a network modifier.[5]

$$\mathrm{NC} = 2 + \frac{No.BOs - No.NBOs}{\text{Total No.Bridging Species}} \quad (1)$$

1.4 Differential Thermal Analysis (DTA)

A combined differential thermal analyser-thermal gravimetric analyser (DTA-TGA) (Stanton Redcroft STA 1640, Rheometric Scientific, Epsom, UK) was used to measure the glass transition temperature (Tg) and the onset crystallization temperature (Tc1) for all glasses. A heating rate of 20^{o}C/min was employed using an air atmosphere with alumina in a matched platinum crucible as a reference. Sample measurements were carried out every 6 s between 30 ^{o}C and 1300^{o}C.was run from 25-1300^{o}C at 20°C intervals.

1.5 Hot Stage Microscope (HSM)

A Misura 3.32 side view hot stage microscope (HSM), Expert Systems (Modena, Italy), with image analysis system and electrical furnace, with max temperature of 1,600 °C and max rate of 80°C/min was used. The parameters for this experiment were a heat rate of 20 °C/min from 20 to 500°C and 5°C / min from 500 to 1,079°C (*Ly-N*), 1126°C (*Ly-C*), 1255°C (*Ly-S*). The computerized image analysis system automatically records and analyses the sample geometry during heating.

1.6 X-ray Photoelectron Spectroscopy (XPS)

X-ray Photoelectron Spectroscopy (XPS) was performed in a Kratos AXIS 165 spectrometer (Kratos Analytical, Manchester, UK) using monochromatic Al Kα radiation (hυ=1486.6 eV). Glass rods with dimensions 15×3ϕ mm mm were produced from the melt and fractured under vacuum (~2×10^{-8} torr) to create pristine surfaces with minimum contamination. Surface charging was minimized by flooding the surface with low energy electrons. The C 1s peak of adventitious carbon at 284.8 eV was used as a charge reference to calibrate the binding energies. High resolution spectra were taken at pass energy of 20 eV,with step size of 0.05 eV and 100ms dwell time. For peak fitting, a mixed Gaussian–Lorentzian function with a Shirely type background subtraction was used.

1.7 Raman Spectroscopy

Raman analysis was conducted on a Witec Confocal Raman Microscope CRM200 equipped with Si detectors, green laser with an excitation wavelength of 532nm and power of 70mW, and a dispersion grating selected of 600l/mm. The instrument was calibrated using

standard silicon including a test run on a focus spectrum. The characteristic Si line at 520 cm^{-1} was maximized through optimization of SMA connector.

1.8 Magic Angle Spinning – Nuclear Magnetic Resonance (MAS-NMR)

^{29}Si MAS NMR spectra were recorded using a 14 T (tesla) Bruker Avance III wide-bore FT-NMR spectrometer (Billerica, MA, USA), equipped with a double broadband tunable triple resonance HXY CP-MAS probe. The glass samples were placed in a zirconia sample rotor with a diameter of 4 mm. The sample spinning speed at the magic angle to the external magnetic field was 10 kHz. ^{29}Si MAS NMR spectra were acquired at 300K with the transmitter set to ~119.26 MHz (-100 ppm) with a 3.0 us pulse length (pulse angle, π /2), 120-second recycle delays, where the signals from 640 scans were accumulated for *Ly-S*, *Ly-C*, and *Ly-N*, respectively. ^{29}Si NMR chemical shifts are reported in ppm, with TMSP (trimethylsilyl propionate) as the external reference (0 ppm). Data were processed using a 25Hz Gaussian apodization function followed by baseline correction.

2. Cell Culture

2.1 Cytotoxicity Analysis

MC-3T3-E1 Osteoblasts (ATCC CRL-2593) were used for this study and were maintained on a regular feeding regime in a cell culture incubator at 37˚C/5% CO_2/95% air atmosphere. Cells were seeded into 24 well plates at a density of 20,000 cells per well and incubated for 24 hours prior to testing. The culture media used was Minimum Essential Medium Alpha Media supplement with 10% fetal bovine serum and 1% (2 mM) L-glutamine (Cambrex, MD, USA).. Glass buttons were incubated in 24 well plates for 24 h and 48 h in Minimum Essential Medium Alpha Media(*n=3/sample/time period*). 100□l of liquid extract was removed (*n=3* per sample well) and these liquid extracts were used for cytotoxicity testing using the Methyl Tetrazolium (MTT) assay. Extracts (100 µl) of sample (*Ly-N*, *Ly-C* and *Ly-S* at 24 h and 48 h) were added into wells

containing MC-3T3-E1 Osteoblasts in culture medium (1 ml) and the 24 well test plates were then incubated for 24 h at 37˚C/5% CO2. The MTT was added in an amount equal to 10% of the culture medium volume/well. The cultures were then re-incubated for a further 2 h (37˚C/5% CO2) after which, the cultures were removed from the incubator and the resultant formazan crystals were dissolved by adding an amount of MTT Solubilization Solution (10% Triton x-100 in Acidic Isopropanol (0.1 n HCI)) equal to the original culture medium volume. Once the crystals were fully dissolved, the absorbance was measured at a wavelength of 570 nm. Control media and healthy growing cell population (*n=3*) were used as a reference.

2.2 Cells Adhesion Procedure

- Glass buttons were washed with 10 volumes of mixture of 50% acetone and 50% ethanol once for 30 min, sonicated in 70% ethanol and rinsed 3 times with 100% ethanol, 30 min each in an orbital shaker at room temperature. Air-dried for 15min.
- Glass buttons were buffered for 72hr by immersing in PBS and shaking at 50 rpm, at 37°C. The solution was exchanged every 8h. pH of the alterations in buffer were monitored until the pH was 7.6-7.85.
- Furthering buffering was carried out in Dulbecco's modified eagle medium for 24h (*n*=3) and 48h (*n*=3). The final pH of buffering medium was 7.4-7.52. Take the media extra for MTT testing.
- Buffered glasses were vacuum-dried for 15min and heated to 120°C for 2h sterilization.

The MC3T3-E1 osteoblast cells were cultured as explained in section 2.7.1. After 48h incubation, media was removed and 5ml trypsin was added to the culture flask. The cells were left to detach for 20 min, after this time, trypsin was removed (centrifuge, 1500rpm, 5 min) and cells were re-suspended in culture media. The trypsin was removed and 10ml media was added. The number of cells was calculated to 20,000 cells per/ml media. The glass buttons were placed in each well where 1ml cell/media solution was seeded onto the surface of the glass buttons and incubated for 24 h (*n=3 per composition*) and 48 h (*n=3 per composition*). Glass buttons were extracted after 24 h and 48.

2.3 Scanning Electron Microscopy (SEM)

- Samples were fixed with 4% (w/v) paraformaldehyde in 1* PBS buffer for 30 min and then post-fixed with 1% osmium tetroxide in distilled water for 1h
- Samples were dehydrated with a series of graded ethanol washes (50/60/70/80/90/100 % I water)
- Samples were immersed in hexamethyldislizane for 5 min and then transferred to a desiccator for 30 min.

Samples' imaging were carried out with an FEI Co. Quanta 200F Environmental Scanning Electron Microscope equipped with an EDAX Genesis Energy-Dispersive Spectrometer. Secondary electron (SE) and backscattered electron (BSE) images were taken as well as.

3. Statistical Analysis

One-way analysis of variance (ANOVA) was employed to compare cell viability of the experimental materials in relation to each composition immersion in media at each individual time period i.e. 24 hours and 48 hours. Comparison of relevant means was performed using the post hoc Bonferroni test. Differences between groups was deemed significant when $p \leq 0.05$.

C. Mechanical Durability of Bioactive Glasses as a Function of Structure, Solubility and Incubation Time

Sample description

Samples used in experiments of this section were sintered to be amorphous and crystalline structures according to the thermal profiles (DTA and HSM). In order to keep amorphous structure of glass, samples were annealed from 25°C to T_g under the heating rate 25°C/min, then kept for 14 hours and cooled with furnace. The crystalline samples were sintered to the sintering temperature determined by HSM.

1. Particle Size Analysis (PSA)

Particle size analysis (PSA) was achieved using a Beckman Coulter Multisizer 4 Particle size analyser (Beckman- Coulter, Fullerton, C.A, USA). The glass powder samples were evaluated in the range of 0.4–100.0 μm and the run length took 60 s. The fluid used was water and was used at a temperature range between 10°C and 37°C. The relevant volume statistics were calculated on each glass.

2. X-ray Photoelectron Spectroscopy (XPS)

X-ray Photoelectron Spectroscopy was performed in a Kratos AXIS 165 spectrometer (Kratos Analytical, Manchester, UK) using monochromatic Al Kα radiation (hυ=1486.6 eV). Glass rods with dimensions 15×3ϕ mm mm were produced from the melt and fractured under vacuum (~2×10−8 torr) to create pristine surfaces with minimum contamination. Surface charging was minimised by flooding the surface with low energy electrons. The C 1s peak of adventitious carbon at 284.8 eV was used as a charge reference to calibrate the binding energies. High resolution spectra were taken at pass energy of 20 eV,with step size of 0.05 eV and 100ms dwell time. For peak fitting, a mixed Gaussian–Lorentzian function with a Shirely type background subtraction was used.

3. Scanning Electron Microscopy (SEM) and EDX

Sample imaging, including those of the original glass powder and glass discs after SBF trials, were carried out with an FEI Co. Quanta 200F Environmental Scanning Electron

Microscope equipped with an EDAX Genesis Energy-Dispersive Spectrometer. Secondary electron (SE) and backscattered electron (BSE) images were taken on glass particles and polished disc surfaces. Electronic Data Systems (EDS) was used to calculate the quantity of compositions of glasses and deposited layers.

4. Ion Release Profiles

Ion concentrations of Sodium ($Na^{+)}$ (*Ly-C*, *Ly-N*), Silicon (Si^{4+}), Titanium (Ti^{4+}), Calcium (Ca^{2+}) and Strontium (Sr^{2+}) (*Ly-S*, *Ly-C*) from water extracts that of glass discs (1.5x8ϕ mm), both amorphous and crystalline, for each formulation (*n*=3) were determined over 1, 7, 30 days using Inductively Coupled Plasma – Atomic Emission Spectroscopy (ICP – AES) on a Perkin-Elmer Optima 5300UV (Perkin Elmer, MA, USA). ICP – AES calibration standards for Ca, Si, Ti and Na/Sr ions were prepared from a stock solution on a gravimetric basis. Three target calibration standards were prepared for each ion and de-ionized water was used as a control.

5. pH Analysis

These water extracts also used for pH Testing. Changes in pH of solutions were monitored using a Corning 430 pH meter. Prior to testing, the pH meter was calibrated using pH buffer solution 4.00±0.02 (Fisher Scientific, Pittsburgh, PA). Sample solutions were prepared by exposing disc samples (*n*=3 amorphous, and *n*=3 crystalline) in calculated quantities of sterile de-ionized water. Measurements were recorded after 1, 7 and 30 days. Sterile de-ionized water was used as a control and was measured at each time period.

6. Hardness Testing

Hardness testing was conducted and glass discs (1.5 x8 ϕ mm). The glass discs used for ICP and pH testing were taken 10 measurements for each of them and 3 discs were used for each composition (total *n*=30/sample). Samples were tested after 1, 7 and 30 days immersion in sterile de-ionized water at 37^{o}C. Each disc (amorphous and crystalline analogues of *Ly-N*, *Ly-C* and *Ly-S*) were mounted in epoxy resin and were lightly polished to remove residual epoxy resin using 600 grit silicon carbide polishing paper. 10 Vickers indentations at a load of 500g and a dwelling time of 15 seconds were made to each disc using a Universal Hardness Machine (HMV-200, Shimadzu, MD, USA). Using the attached light microscope and computer, the diagonals created

by the Vickers diamond indenter were measured and the VHN was calculated using equation 2, where F = the applied load (kgf), d = diagonal length (mm).

$$H=1.854\frac{F}{d^2} \qquad (2)$$

D. Simulated Body Fluid and Cytocompatibility of the Glasses

In this section, the sintered glass powder discs were used to do SBF trials. In order to keep amorphous structure of glass, samples were annealed from 25°C to T_g under the heating rate 25°C/min, then kept for 14 hours and cooled with furnace. The crystalline samples were sintered to the sintering temperature determined by HSM.

1. Simulated Body Fluid Testing (SBF)

Table IV. The Compositions of SBF

Order	Reagent	Required amount (g)
1	NaCl	7.996
2	$NaHCO_3$	0.35
3	KCl	0.224
4	$K_2HPO_4 \cdot 3H_2O$	0.228
5	$MgCl_2 \cdot 6H_2O$	0.305
6	1 M·HCl	40ml
7	$CaCl_2$	0.278
8	Na_2SO4	0.071
9	$NH_2C(CH_2OH)_3$	6.057

Simulated body fluid (SBF) was produced in accordance with the procedure outlined by Kokubo *et al*.[43] The compositions of SBF were presented in Table 4. The reagents were dissolved in order, from reagent 1–9, in 500 ml of purified water using a magnetic stirrer. The solution was maintained at 36.5°C. 1 M·HCl was titrated to adjust the pH of the SBF to 7.4. Purified water was then used to adjust the volume of the solution up to 1 L. Heat treated discs (n = 3/sample) were immersed in concentrations of SBF determined by Vs=Sa/10 (Vs = volume of extract used and Sa = exposed surface area of the disc) and subsequently incubated for 1, 7 and 30 days at 37°C. A JOEL JSM-840 scanning electron microscope equipped with a Princeton Gamma Tech (PGT) Energy Dispersive X-ray (EDX) system was used to obtain secondary electron images and carry out chemical analysis of the surface of these glass discs. All EDS spectra were collected at 20 kV,

using a beam current of 0.26 nA. Quantitative EDS converted the collected spectra into concentration data by using standard reference spectra obtained from pure elements under similar operating parameters.

2. Cell Culture

The established cell line L-929 (American Type Culture collection CCL 1 fibroblast, NCTC clone 929) was used in this study as required by ISO10993 part 5. Cells were maintained on a regular feeding regime in a cell culture incubator at 37˚C/5% CO2/95% air atmosphere. Cells were seeded into 24 well plates at a density of 10,000 cells per well and incubated for 24 hours prior to testing with extracts. The culture media used was M199 media (Sigma Aldrich, Ireland) supplemented with 10% foetal bovine serum (Sigma Aldrich, Ireland) and 1% (2 mM) L-glutamine (Sigma Aldrich, Ireland). The cytotoxicity of the glass extracts was evaluated using the Methyl Tetrazolium (MTT) assay in 24 well plates. Aliquots (100 µl) of undiluted sample were added into wells containing L929 cells in culture medium (1 ml) in triplicate over 1, 7 and 30 days. The plates were incubated for 24 h at 37˚C/5% CO2. The MTT assay was then added in an amount equal to 10% of the culture medium volume/well. The cultures were then re-incubated for a further 2 h (37˚C/5% CO2). Next, the cultures were removed from the incubator and the resultant crystals were dissolved by adding an amount of MTT Solubilization Solution (10% Triton x-100 in Acidic Isopropanol. (0.1 n HCI)) equales to the original culture medium volume. Once the crystals were fully dissolved, the absorbance was measured at a wavelength of 570 nm.

3. Statistical Analysis

One-way analysis of variance (ANOVA) was employed to compare the changes in ion release, cell culture, pH and hardness of the experimental materials in relation to 1) maturation of each composition and structure (amorphous and crystalline) over 1, 7 and 30 days immersion in sterile de-ionized water, 2) differences in structure i.e amorphous and crystalline at each individual time period i.e. 1 day, 7 day and 30 day. Comparison of relevant means was performed using the post hoc Bonferroni test. Differences between groups was deemed significant when $p \leq 0.05$.

III. RESULTS AND DISCUSSION

A. Effect of Na+ and Sr2+ on the Structure and Biocompatibility of the Glasses

The series of bioactive glasses in this project contain three compositions: *Ly-N* is Na-containing glass, *Ly-C* is the intermediate glass composed of both Na and Sr, *Ly-S* is Sr-containing glass. The specific compositions are shown on Table III. X-ray fluorescence (XRF) analysis has been widely used to determine composition of major and trace elements in glass and the results were very credible. XRF was used in this project to determine the compositions of the glass series. Table V shows the XRF data indicating that actual compositions of the glasses are comparable to the batch compositions of the glass series.

Table V. Glass composition (mol fr) , and Composition Determined by XRF

	Ly-N		***Ly-C***		***Ly-S***	
	Composition	***XRF***	***Composition***	***XRF***	***Composition***	***XRF***
SiO_2	*0.55*	*0.53*	*0.55*	*0.53*	*0.55*	*0.56*
CaO	*0.22*	*0.23*	*0.22*	*0.23*	*0.22*	*0.22*
TiO_2	*0.05*	*0.05*	*0.05*	*0.05*	*0.05*	*0.05*
Na_2O	*0.18*	*0.18*	*0.09*	*0.09*		
SrO			*0.09*	*0.09*	*0.18*	*0.17*

Network calculations were performed on the basis of Eq.1 assuming that Ti^{4+} acts as both a network former and a network modifier. Previous studies has proven that Ti^{4+} can either act as a network former in four-fold coordination like Si^{4+} or a network modifier in a six-fold coordination state.[17] When Ti was considered as a network former, the a NC of 2.36 for each glass was determined by theoretical calculation, while a NC of 2.26 for *Ly-N* and *Ly-C* and a NC of 2.42 for *Ly-S* were determined on the basis of XRF data. The value of NC is proportional to the concentration of Si^{4+}. This fact explains the slight difference between the values of NC based on the starting compositions of glass series and those determined by XRF. When Ti^{4+} was considered as a network modifier, the theoretical calculation presented a NC of 2.67 for each glass, while a NC of 2.58 for *Ly-N* and *Ly-C* and a NC of 2.72 for *Ly-S* were determined on the basis of XRF results. It has been reported that glasses that have NC greater than 2.4 are not likely to be bioactive. Previous studies reported that NC affects HCA formation on SiO_2-CaO-Na_2O glass discs in

simulated body fluid (SBF). Above NC of 2, the rate of HCA layer deposition decrease rapidly.[6] Therefore, the results of ion release profiles and SBF will present whether the Ti^{4+} acts as a network former or a network modifier.

Fig 8(a) shows XRD patterns of the series of glasses. The relatively smooth curves identified the amorphous nature of each glass. Figure 8(b) shows the DTA profiles of the glasses series. The glass transition temperature (T_g) of *Ly-N* was found to be 591°C, the first crystallization peak (T_{c1}) started at 777°C. The T_g of *Ly-C* and *Ly-S* are respectively 650°C and 760 °C, and T_{c1} of them are 778°C and 871°C. Glass discs were heated under their T_g to retrieve amorphous structure. The sintering temperature determined by HSM is the basis of heat treating temperature of crystalline samples (653°C for *Ly-N*, 713°C for *Ly-C*, 825°C for *Ly-S*).

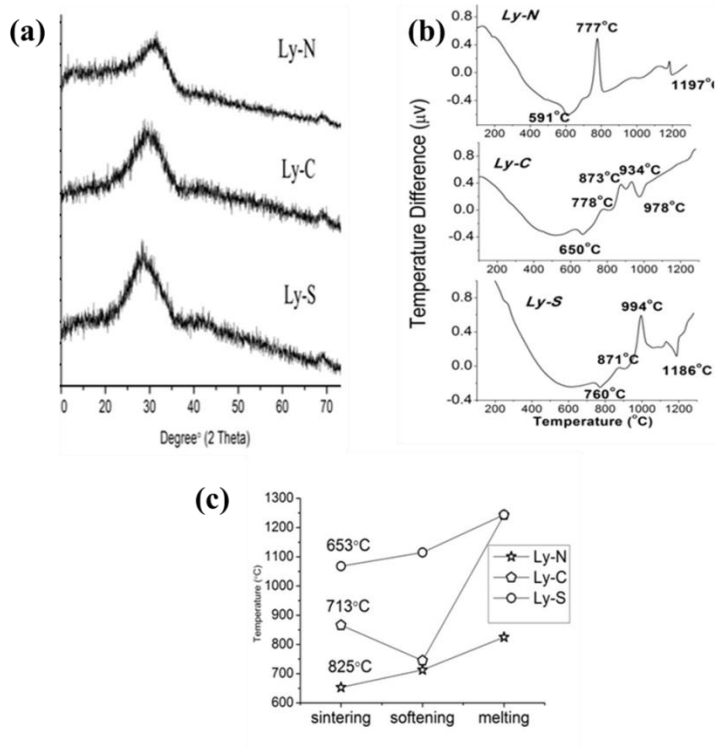

Figure 8. (a) XRD images and (b) Thermal profile of the series of glasses.(c) The HSM profile of the glass series.

Raman spectroscopy is very sensitive to changes in the Si–O–Si environment of silica based glasses with different compositions. It is also a technique employed for the identification of Si–O–NBO bonds in bioactive glasses.[50] It was conducted on each glass and the resulting spectra are

shown in Figure 9. All three glasses presented the similar bands at 344 cm^{-1} and approximately 605 cm^{-1}. Based on the nomenclature first introduced by Bell *et al.*[40], the lowest frequency band was associated with a bond-rocking vibration, in which the oxygen atoms move perpendicular to the Si–O–Si plane. The rocking vibrations identified at 560–620 cm^{-1} are associated with Si-O-Si structure. According to these facts, *Ly-N*, *Ly-C* and *Ly-S* have very similar Si-O-Si structures. A slight shift of peaks in wavenumber occurred within the range of 800-1000 cm^{-1}: the spectrum of *Ly-N* presented a peak at 873 cm^{-1} within a narrower spectral region (900-1000 cm^{-1}) compared to those of *Ly-C* and *Ly-S*. The absorption bands of *Ly-C* and *Ly-S* occurred respectively at 861 cm^{-1} and 852 cm^{-1}. It has been proved that the anti-Stokes line at 860 cm^{-1} is related to the presence of the Si–O–NBO bonds in glassy network and so are the peaks ranging from 900 to 1000 cm^{-1} (peaks between 950-1000 cm^{-1} are associated with symmetrical stretching motion in Q_2, the peak at 900 cm^{-1} are associated with Q_1).[51] Q_n is used to characterize the distribution of NBOs over the tetrahedral structure units, where n refers to the number of bridging oxygen atoms surrounding the tetrahedron. Therefore, the series of glasses have similar Si-O-NBO structures. The narrow spectral region (900 -1000 cm^{-1}) of *Ly-N* might represent slightly higher intensity of Si-O-NBO.

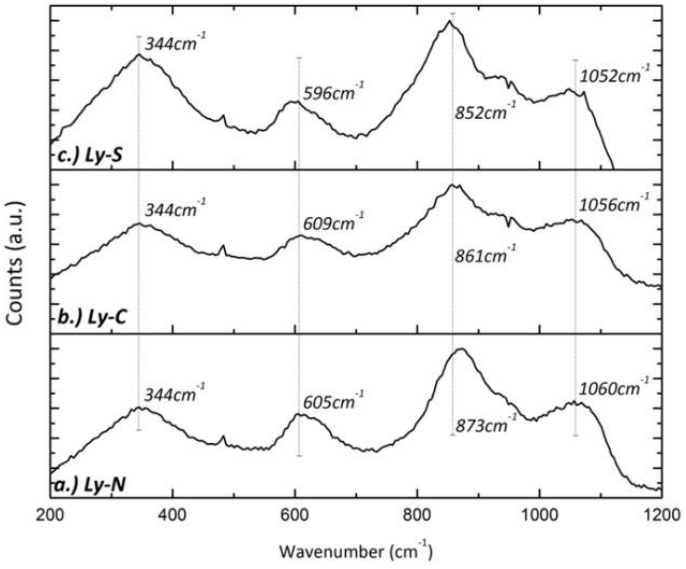

Figure 9. Raman spectroscopy of the series of glasses.

High resolution X-ray photoelectron spectroscopy (XPS) was conducted on the series of glasses and the O 1s signals are shown in Figure 10. These O1s peaks provide very useful information because the oxide ions in the silicate glasses have different type of chemical bonding[52]. Then, it is possible to analyze the bonding states of the oxide ions by deconvoluting the O1s spectrum. The two peaks of *Ly-N* are at binding energies of 529.7 eV and 531.3 eV respectively which are representative of NBO and BO concentrations. The peaks of *Ly-C* present at binding energies of 529.9 eV and 531.6 eV respectively which are slightly higher than those of *Ly-N*. The peaks of *Ly-S* shifted to higher binding energies of 530.1 eV and 531.8 eV. Irrespective of compositions, the ratio of BO/NBO of the series of glasses is consistent as 0.82 (Table I in Appendix) indicating that Na^+ and Sr^{2+} are both structural modifiers. However, the ratio of BO/NBO of *Ly-N* (0.81) is little lower than that of *Ly-C* (0.87) and *Ly-S* (0.84). This fact suggests that *Ly-N* has slightly higher NBO concentration, which confirms the result of Raman.

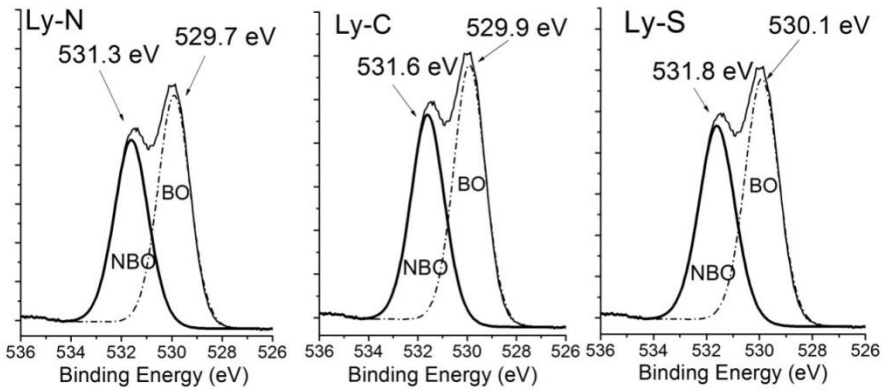

Figure 10. XPS high resolution O 1s of *Ly-N*, *Ly-C* and *Ly-S*.

The results of magic angle spinning-nuclear magnetic resonance (MAS-NMR) are shown in Figure 11. MAS-NMR spectroscopy has played an important role in the development of structural and dynamical models of glass structure. The chemical shift is a sensitive probe of the local environment of a given isotope, like ^{29}Si used in this project, hence providing an inventory of the species present. The chemical shift of an individual nucleus is dependent on the shielding of the nucleus (the local electron density which in turn reflects the distribution of other atoms about the nucleus).[53] *Ly-N* exhibited a peak at -84.12ppm. The peaks of *Ly-C* and *Ly-S* were at -84.8ppm and -85.09ppm respectively. It has been reported that peaks of ^{29}Si spectrum appear at approximately 84ppm spectrum are ascribed to Q_2 species[54] containing two NBOs. In addition, the

small shift of *Ly-N* occurred at lower frequencies indicated slightly higher concentration of NBOs which is consistent as results of XPS and Raman.

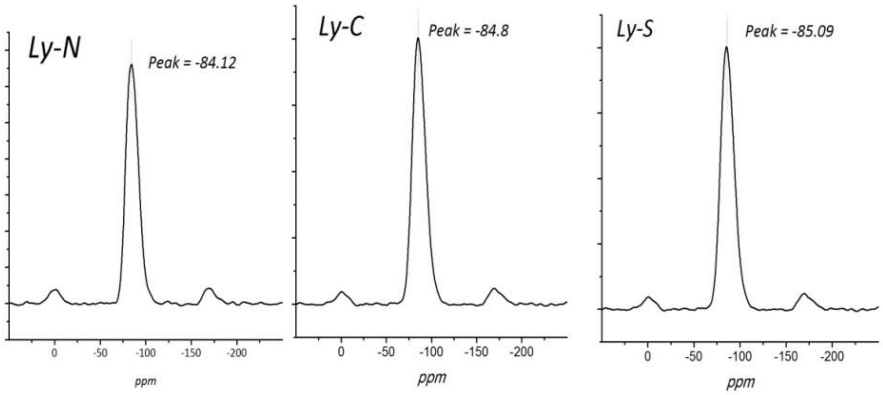

Figure 11. MAS-NMR spectra of *Ly-N*, *Ly-C*, *Ly-S*.

Bioactive glasses can create a novel microenvironment due to the ionic dissolution products released into the culture medium. This microenvironment will modify the growth and adhesion of osteoblast to these biomaterials.[55] If the ion concentration is high enough, it will not only influence the adhesion of cells but also can kill the cells. This is why the cell viability is necessary to be tested. Figure 12 shows the results of cell viability testing conducted on the extracts of pure glass buttons which were used in the cell culture testing soaking in the medium for 24h and 48h.

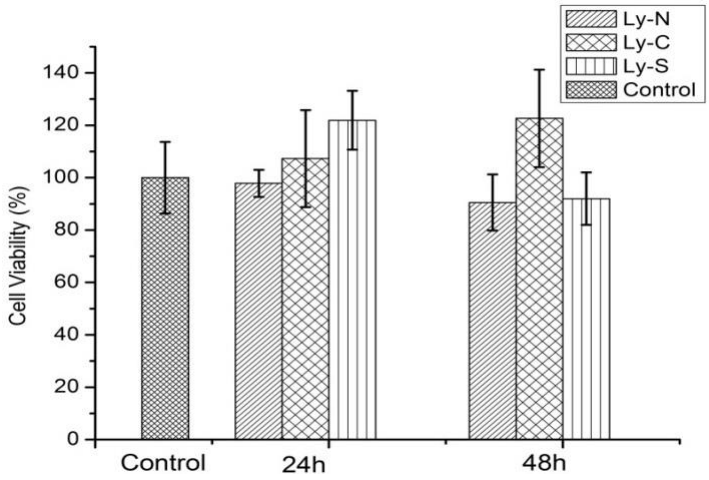

Figure 12. Cell viability from pure glass buttons extracts in 24 hours and 48 hours.

Compared to the control group (cells in the media without adding the extracts), there is no difference in the cell viability with each glass extract after 24 hours (p=0.720-1.000) and 48 hours

(p=0.480-1.000). This fact confirms the series of glasses are compatible. In addition, it can be observed that the extracts from *Ly-C*, *Ly-S* after 24 hours and *Ly-C* after 48 hours increase the cell viability. The positive influence of Sr^{2+} on the osteoblast cells can explain the phenomena. Previous study about a group bioactive glass (compositions: 46.46 SiO_2 – 1.07 P_2O_5 – 26.38 Na_2O – 23.08 (SrO:CaO) (mole %) where either no calcium (0%) or 10, 50 or 100% of the Ca was substituted with Sr) reported that significantly higher (osteoblast) cell viability activity of 100% Sr-substituted sample (SiO_2–P_2O_5–Na_2O–CaO) than that in any other group.[56]

The SEM images of osteoblast cells on surface of *Ly-N*, *Ly-C* and *Ly-S* after incubating for 24h are shown in Figure 13-15. The image with 200× magnification of each sample shows obviously that cells attached on surface. Images with higher magnification provide clear special morphology of cells. The morphology of cells attached on the surface of *Ly-N* is some rounded and less spread out compared to that of cells attached on the surface of *Ly-C* and *Ly-S*. Cells attached on the surface of *Ly-S* appeared more flat shape and the cellular edge formed larger lamellipodia ending with filopodia. The lamellipodia with filopodia present the spreading of cells. The morphology of these mice osteoblast cells look very similar with that of primary human osteoblast cells attached on the surface of polished titanium after incubating for 24h.[57]

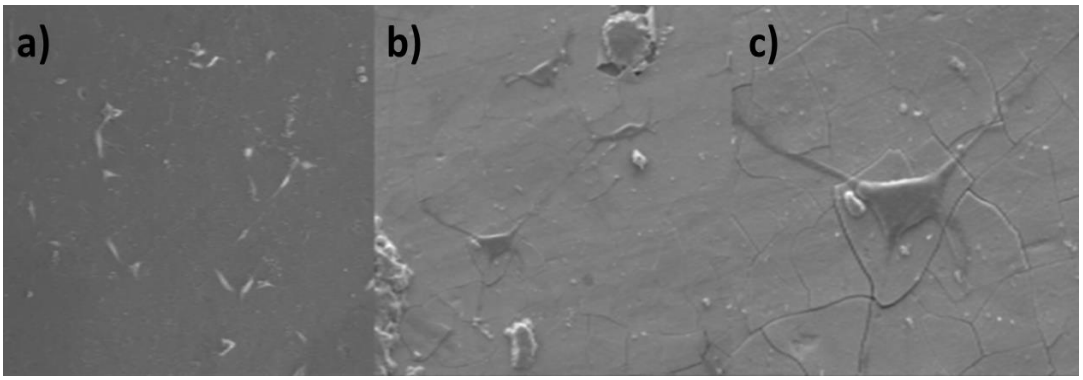

Figure 13. The SEM images of cells attached on the surface of *Ly-N* after 24h with a) 200×, b) 400× and, c) 1000 × magnification.

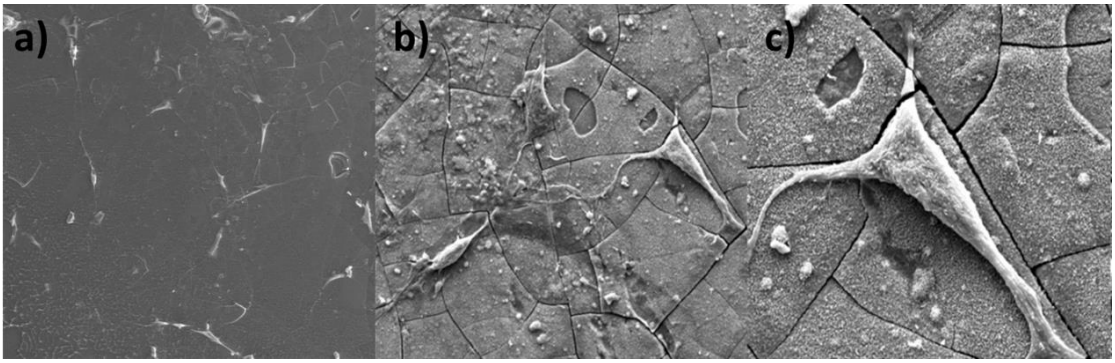

Figure 14. The SEM images of cells attached on the surface of *Ly-C* after 24h. with a) 200×, b) 1000× and c) 2811 × magnification.

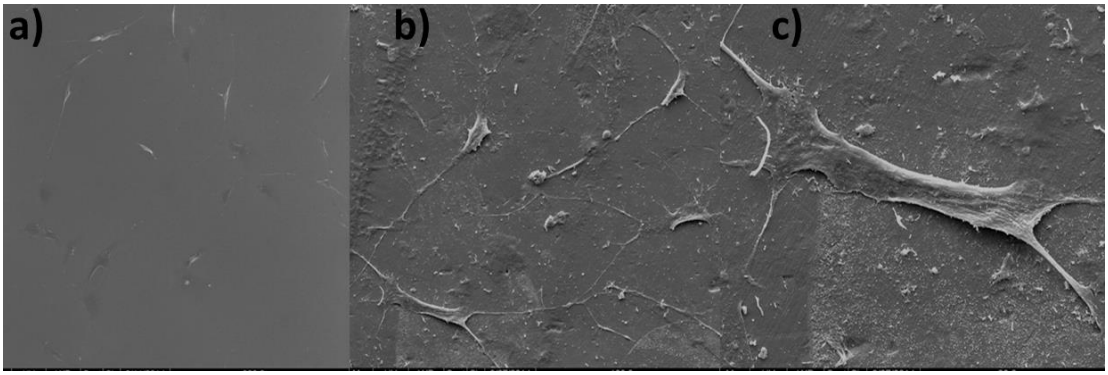

Figure 15. The SEM images of cells attached on the surface of Ly-S after 24h with a) 200×, b) 500× and c) 1542 × magnification.

A previous study reports that cells attached on the surface of bioactive glass just after 3h appeared spherical morphology almost without filopodia which anchors the cells on the surface of samples[58]. In addition, instead of "individual dot" adhesion observed on the surface of *Ly-N*, cell-cell contact by filopodia started to appear on the surface of *Ly-C* and *Ly-S*. The fact that Sr^{2+}can enhance the replication of preosteoblastic cells and stimulate bone formation in cell cultures *in vitro*[23] can explain why the adhesion and spread of cells on the surface of Sr-containing samples is better.

The SEM images of cells on surface of *Ly-N*, *Ly-C* and *Ly-S* after incubating for 48h are shown in Figure 16-18. Images of each sample with 200× magnification indicate more cells attached on the surface of each sample after 48h compared to that of 24h. For *Ly-S*, images with 100× were selected instead of image with 200×, because it can better reveal that the surface of *Ly-S* is greatly covered by cells. Besides, more cell-cell contact can be observed. Some cells which were plated and reached confluence, parallel and arranged in a polarized monolayer can be

observed on the surface of all samples. Figure 16 shows that cells adhered on the surface of *Ly-N* started to grow filopodia, and the cell-cell contact as well as can be observed. The morphology of cells attached on the surface of *Ly-C* ad *Ly-S* looks like that of primary human osteoblast cells attached on the polished titanium after 7 days.[57] The fact presents that the spread of cells went well for all samples, in other words, the series of glasses are able to provide friendly environment for cells to adhere and spread. To compare the morphology and concentration of cells attached on the surface of the glass series after 24h and 48h, more cells can be observed and these cells spread out with more and larger filopodia resulting in better cell-cell contact. Therefore, it is reasonable to hypothesize that cell attachment and adhesion will perform better after longer incubation periods.

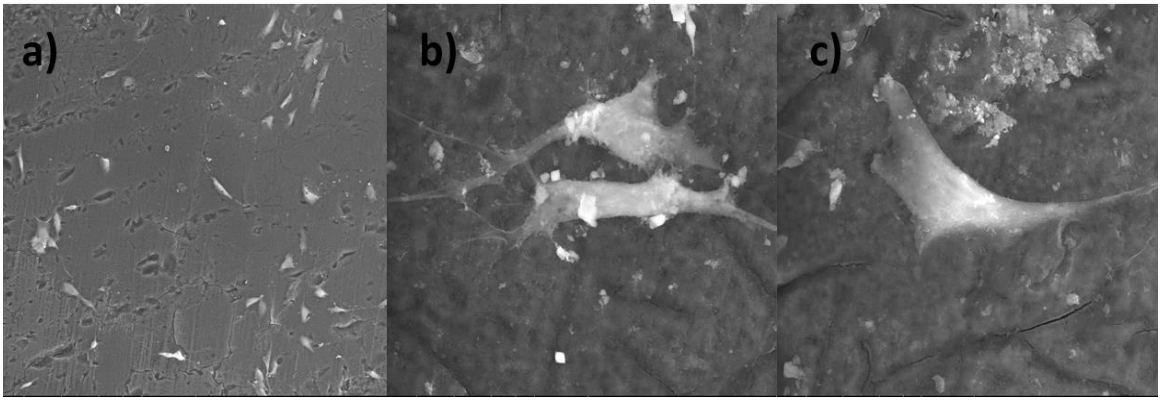

Figure 16. The SEM images of cells attached on the surface of *Ly-N* after 48h with a) 200×, b), c) 2000× magnification.

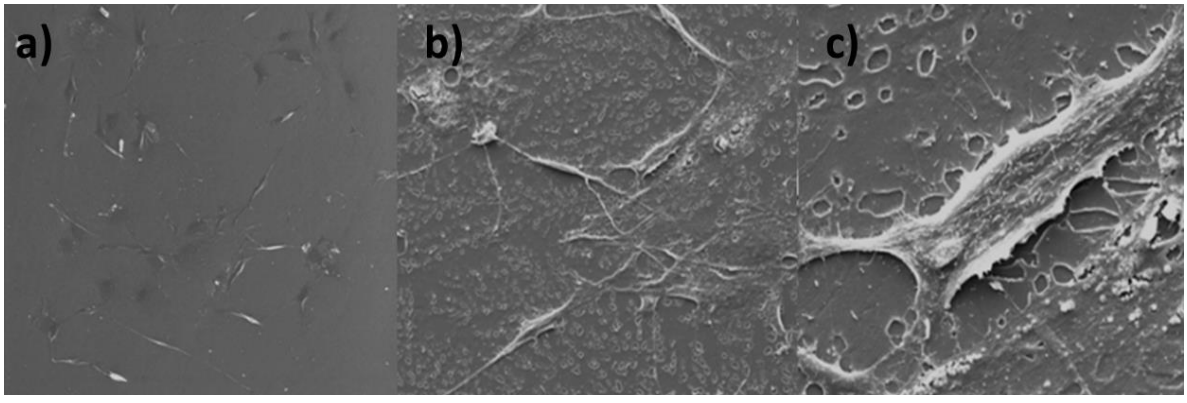

Figure 17. The SEM images of cells attached on the surface of *Ly-C* after 48h with a) 200×, b) 500× and c) 2500 × magnification.

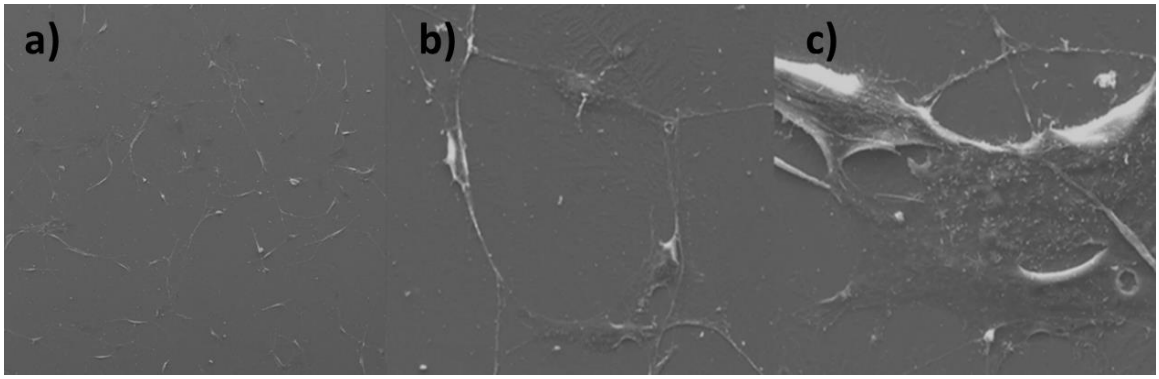

Figure 18. The SEM images of cells attached on the surface of *Ly-S* after 48h with a) 200×, b) 700× and c) 2500 × magnification.

Section Summary

This section employed characterization techniques to demonstrate that the series of glasses (*Ly-N*, *Ly-C* and *Ly-S)* have similar atomic structure, as Sr^{2+} and Na^{+} both act as glass network modifiers. Additionally, the results of cell viability show that *Ly-N*, *Ly-C* and *Ly-S* do not have a negative influence on the viability and adhesion of the osteoblast cells. After soaking in the medium for 24h, the extracts of *Ly-C* and *Ly*-S increase the adhesion of these cells. The extract of *Ly-C* after 48h presented the same positive influence on osteoblast viability. The SEM images of cell attachment presents that all the samples support the cell adhesion, which indicates that the biocompatibility and bioactivity of the series of glasses is favorable. More filopodia, flatter morphology and cell-cell contact of cells attached on the surface of Sr-containing (*Ly*-C and *Ly-S*) samples indicates that Sr^{2+} has a positive effect on the adhesion of these cells to the glass surface compare to the Na^{+} glass. The following section is conducted to evaluate the solubility and mechanical durability of each glass as a function of atomic structure and incubation time in an aqueous environment.

B. Mechanical Durability of Bioactive Glasses as a Function of Structure, Solubility and Incubation Time

X-ray photoelectron spectroscopy (XPS) can determine the intrinsic binding energy of the atomic orbitals, which shifts chemically according to the surroundings of the atoms. It has been extensively applied to the interpretation of the structure, electronic state and composition of glass. XPS was conducted on each glass to confirm the compositions of the starting glasses. The results are shown in Figure 19 and Table VI. Figure 19 presents the survey scan of *Ly-N* containing Na, O, Ti, Ca, Si and minor traces of carbon (C). The survey scan of *Ly-C* showed that it contains Na, O, Ti, Ca, Si, Sr and slight amount of C. The survey of *Ly-S* contained Si, O, Ti, Ca, Sr and also traces of C. The composition of each glass was analyzed on a fracture surface in a pristine environment by XPS to confirm the compositions of starting glass. Table 6 revealed the compositions of the starting glasses and the compositions determined by XPS. An excess of Na_2O determined by XPS in *Ly-N* and *Ly-C* can be observed in Table 6. This possibly attributes to the fact that, as a mobile ion, Na^+ tends to migrate to fracture/exposed surface on glass.[5]

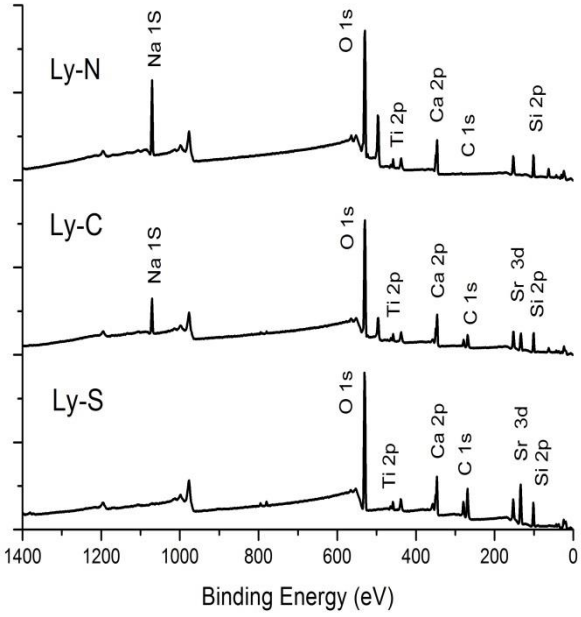

Figure 19. XPS survey scan of *Ly-N*, *Ly-C*, *Ly-S*.

Table VI. The Compositions (mol fr) of Starting Glasses and Detected by XPS

	Ly-N		***Ly-C***		***Ly-S***	
	Composition	***XPS***	***Composition***	***XPS***	***Composition***	***XPS***
SiO_2	*0.55*	*0.52*	*0.55*	*0.51*	*0.55*	*0.54*
CaO	*0.22*	*0.22*	*0.22*	*0.23*	*0.22*	*0.23*
TiO_2	*0.05*	*0.03*	*0.05*	*0.04*	*0.05*	*0.04*
Na_2O	*0.18*	*0.23*	*0.09*	*0.13*		
SrO			*0.09*	*0.09*	*0.18*	*0.19*

The glass particle size was analyzed by Scanning Electron microscopy (SEM) and Particle Size Analysis (PSA). The results are shown in Figure 20. PSA presented the mean particle size of the series of glasses: 4.6 μm for *Ly-N*, 3.9 μm for *Ly-C* and 4.6 μm for *Ly-S*, which are comparable to the particle sized determined by SEM imaging (3.9-4.5 μm).

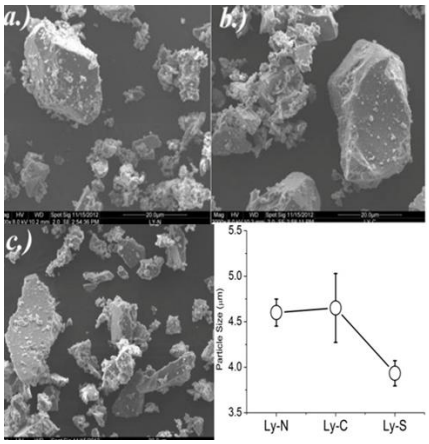

Figure 20. SEM images of a)*Ly-N*, b) *Ly-C*, c) *Ly-S* glass particles and particle size analysis data. of the glasses.

The relatively smooth curves of XRD patterns shown in Figure 21(a) confirmed the amorpous structure of the series of glasses, and Figure 21(b) shows the corresponding crystalline analogues after heating treatment, the anealing temperaures were determined by the thermal profiles (HSM). The major crystal phase of both *Ly-N* and *Ly-C* (Table II in Appendix) is $Na_2Ca_2Si_3O_9$ that is also the principal crystal phase of Bioglass®[59]. The primary crystal phases of *Ly-S* (Table II in Appendix) are Sr_2Si_3, Ti_8O_{15}, $CaSi_2$ and $Sr_2TiSi_2O_8$. It has been reported that the crystalline structure of glass-ceramics decrease their biosolubility and bioactivity.[60]

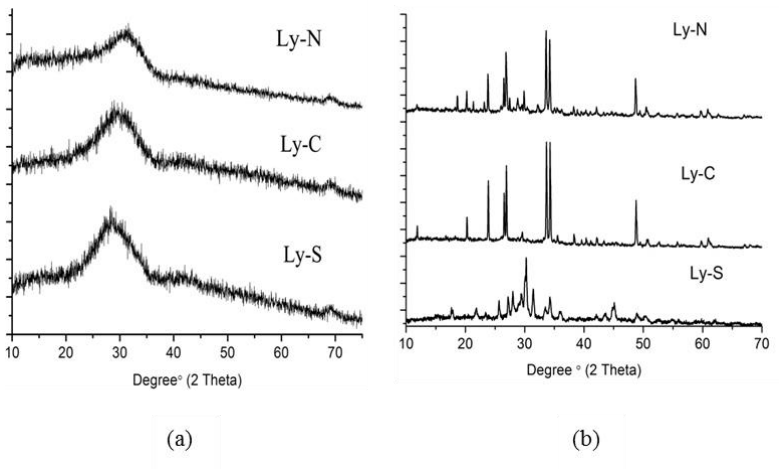

Figure 21. XRD patterns of *Ly-N*, *Ly-C* and *Ly-S*: (a) amorphous and (b) crystalline structure.

An important attribute of bioactive glasses is that the local microenvironment will be influenced significantly by the dissolution products of the materials. pH will increase due to leaching and dissolution of alkalis and alkaline earths from bioactive glasses[61] like Na^+ and Ca^{2+}. According to the bioactive process, the first stage for CaP/HCA formation in SBF is the rapid cation exchange of network modifier, like Na^+ and Ca^{2+}, with H^+ coming from the solution creating silanol bonds (Si-OH) on the glass surface: $Si\text{-}O\text{-}Na^+ + H^+ + OH^- \quad Si\text{-}OH \rightleftharpoons Na^+(aq) + OH^-$. In addition, the Na^+/H^+ ion exchange results in increase local alkalinity and further hydrolysis (breaking of Si-O-Si bonds) of glass network[48]. Ca^{2+} enables to facilitate the formation of CaP or HCA films. Therefore, it can be conjectured that the samples with higher concentration of Na^+ and Ca^{2+} determined by ICP testing have higher pH values and form CaP or HCA deposited layers more effectively, which can be verified by SBF trials. Silicic acid ($Si(OH)_4$) has been shown to simulate collagen I production by human osteoblast cells at a concentration of 10 mmol. 45S5 Bioglass® with 15-20 µg/ml of soluble Si promoted highest metabolic activity of mature osteoblasts and enhanced formation of mineralized bone nodules.[11] Sr^{2+} is reported to promote the bone cell proliferation and new bone formation, and at the same time reduce bone resorption.[62]

In this section, ion release profiles were estimated for both the amorphous and crystalline samples with respect to maturation time which is the basis of statistical comparisons (Table VII.(a)). The statistical comparisons were also conducted by comparing ion releasing as a function of amorphous/crystalline structure (Table VI.(b)). Ion release rates of overall amorphous samples are much higher than those of samples with crystalline structure evidently shown in Figure 23. This fact was confirmed by the statistical analysis, in particular for Na^+ and Si^{4+} ($p \leq 0.05$). When

ion release rates for each individual ion from amorphous samples were compared with respect with maturation time, Na^+ and Si^{4+} also experienced a significant difference ($p \leq 0.05$), whereas Ca^{2+} didn't ($p \geq 0.05$). Na^+ is structural modifier breaking the Si-O-Si network, resulting in glasses with high level of solubility and bioactivity. The highest Na^+ concentration (216 µg/mL, *Ly-N*) is similar to another Na-containing bioactive glass (Ca-Sr-Na-Zn-Si) which ranged from 190 to 270 µg/mL, but the highest Si^{4+} concentration (172 µg/mL, *Ly-N*) is much higher than Si^{4+} released from Bioglass® which was 43 µg/mL after 30 days.[63] Therefore, *Ly-N* with amorphous structure is expected to have better performance in SBF trials. Concentrations of Ca^{2+} released from amorphous *Ly-C* and *Ly-S* increased to the same maximum 17.9 µg/mL after 30 days which is higher than that of another Sr-containing bioactive glass[56] (a bioactive glass series (SiO_2–P_2O_5–Na2O–CaO) in which 0–100% of the Ca was substituted by Sr) (9.1 µg/mL), however, this is similar to that of Bioglass® (17 µg/mL). Sr^{2+} has the same charge and very similar ionic radius as Ca^{2+}, which enables direct substitution. Therefore, Sr^{2+} possibly partially fulfills the role of Ca^{2+} as a charge compensator.[56] These facts explain why the glasses with addition of Sr^{2+} have higher concentrations of Ca^{2+}.

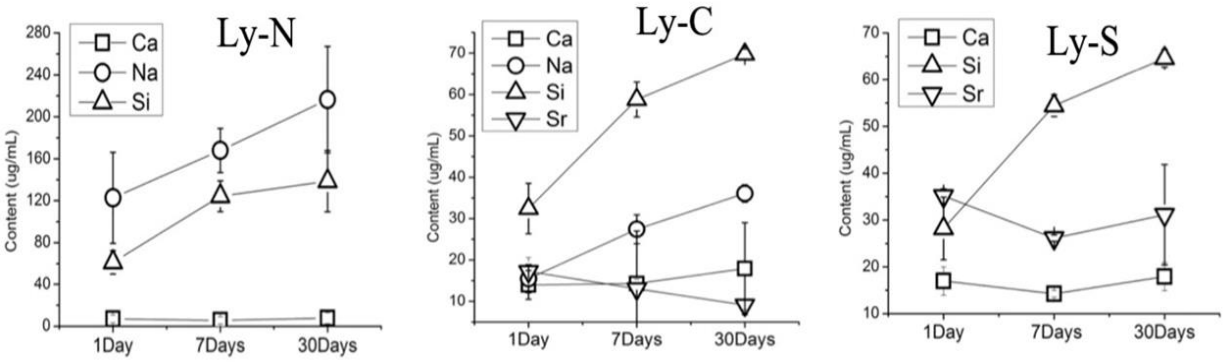

Figure 22. Ion release profiles of amorphous samples.

Ion release profiles of the crystalline samples are presented in Figure 23. The ion concentrations of the crystalline samples are much lower than those of the amorphous ones. Previous studies reported that slower ion release and lower ion concentrations of Na_2O-containing SiO_2-CaO bioactive glass-ceramics.[60,64] The Si-O-Si bonds in the regular long-ranged structure of crystalline samples are difficult to be broken by water molecules.

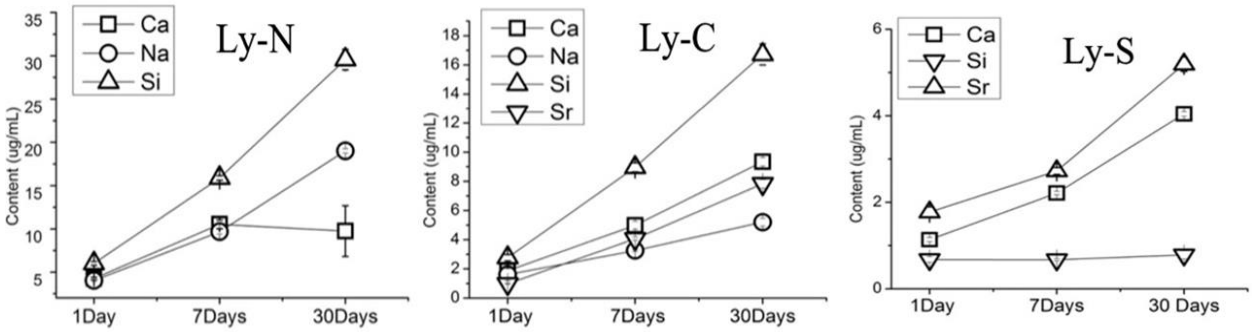

Figure 23. Ion release profiles of crystalline samples.

Table VII. Means Comparison of Each Ion Release Profile At 1 Day, 7 Days And 30 Days With Respect Structure, and Just With Respect to Maturation Time

		(a)Amorphous vs. Crystalline			(b) Maturation
		1Day	**7Days**	**30Days**	**1Day vs. 30Days**
Ly-N	**Ca**	0.259	0.070	0.201	1.000
	Na	0.009	0.000	0.003	0.001
	Si	0.001	0.000	0.003	0.010
Ly-C	**Ca**	0.004	0.274	0.252	1.000
	Na	0.002	0.000	0.000	0.001
	Si	0.001	0.000	0.000	0.000
	Sr	0.001	0.003	0.132	0.020
Ly-S	**Ca**	0.001	0.000	0.001	1.000
	Si	0.002	0.000	0.000	0.000
	Sr	1.000	0.000	0.014	1.000

With respect to the maturation time (1 Day vs. 30 Days), there was significant increase in pH for *Ly-N*, *Ly-C* and *Ly-S* with both amorphous and crystalline structure (p=0.000, 0.002 (*Ly-S*)). When structure (amorphous/crystalline) was considered as the primary influencing factor, pH values for every sample at each time period experienced significant changes (p=0.000) (Figure 24).

For bioactive glasses, possessing both good bioactivity and mechanical properties is a persistent challenge due to the uncertainty related to their chemo-mechanical (changes in mechanical properties due to reactions with a biological environment) behavior and mechano-chemical (effect of mechanical strain on dissolution rate) behavior. Therefore, there still exists a lack of understanding of the relationship between the mechanical properties of bioactive glasses and their bioactivity. In this project, hardness testing was conducted for determining any changes

in mechanical durability as a function of incubation time in an aqueous environment, and also as a function of amorphous/crystalline structure.[64]

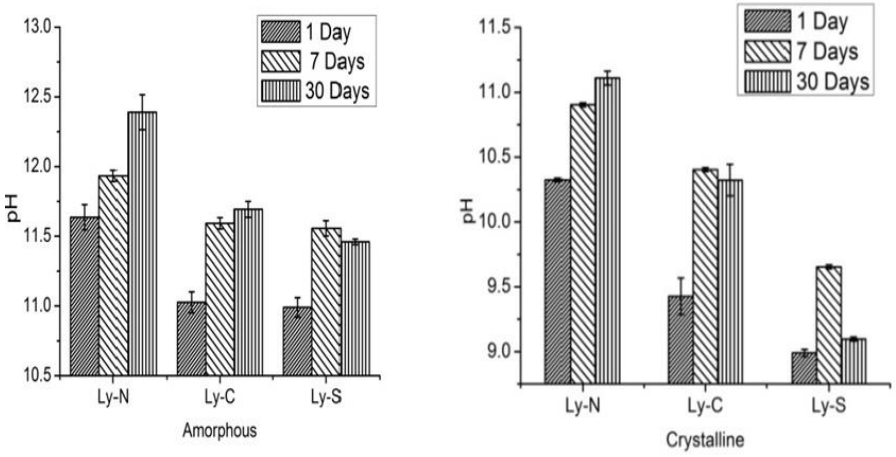

Figure 24. pH of extracts from both amorphous and crystalline samples with respect to maturation i.e. after 1, 7 and 30 days.

Due to the high level reactivity between the series of bioactive glasses and the aqueous environment concluded from the results of ion release profiles, the hardness was expected to vary along with the incubation time. Results of hardness testing are shown in Figure 25, was estimated to determine any change in mechanical durability as a function of incubation time. Significant deductions in strength (GPa) after 30 days of each amorphous sample compare to 1 day can be observed in Figure 25: from 2.6 to 1.0 GPa for *Ly-N*, from 3.0 to 0.9 GPa for *Ly-C*, from 3.4 to 1.8 GPa for *Ly-S*. The reduction of hardness is ascribed to dissolution of the glasses proven by the ion release profiles and pH testing. On the contrary, the crystalline samples did not experience significant reduction in hardness. The highest value of hardness belonged to crystalline *Ly-C* (6.0 GPa). Hardness value of *Ly-S* with crystalline structure (4.7 GPa) is higher than that of crystalline *Ly-N* (2.0 GPa). The addition of Sr^{2+} is one of the possibilities influencing this effect.

Previous studies have proven that the addition of strontium oxide enhances the compressive strength of the glass-ionomer cements.[65] The existence of Na^{+} is also able to cause this phenomenon. A liner relationship exists between T_g and hardness of a bioactive glass. A decrease of T_g of a bioactive glass predicts that the glass has reduced hardness. A similar relation between T_g and the hardness of a bioactive glass was explained by Baesso *et al* (1999). T_g is reduced when

Na_2O content is increased.[66] In other words, the concentration of Na^+ of a bioactive glass is in inverse proportion to its hardness. This fact explains why *Ly-N* has lower values of hardness.

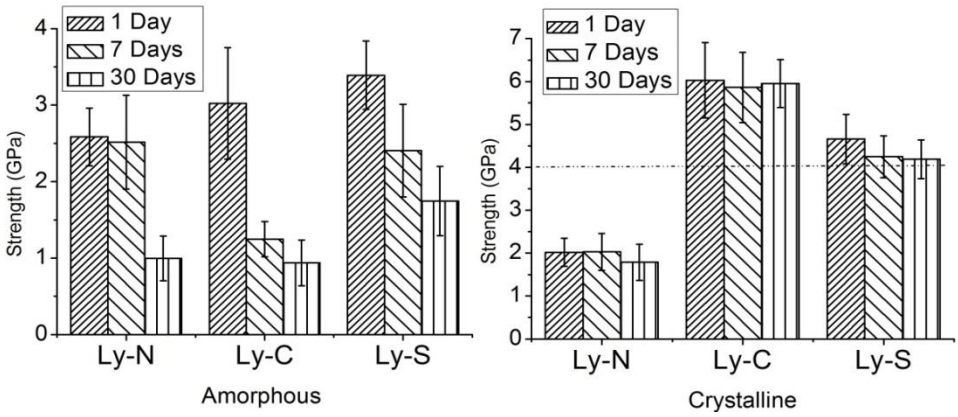

Figure 25. Hardness testing of sintered discs from both amorphous and crystalline samples.

Section Summary

It can be concluded that the amorphous samples released more ions with a corresponding enhancement of pH values than the crystalline samples. The crystalline materials performed better mechanically in an aqueous environment with respect of time, while the amorphous material experienced a significant reduction in hardness over time. These facts suggest that the crystalline structure can control the solubility and improve the mechanical durability of glass/glass-ceramic materials. The following section will determine the bioactivity of the amorphous and crystalline samples in a synthetic physiological fluid (Simulated Body Fluid, SBF) as a function of incubation time, in this case, 1, 7 and 30 days.

C. Simulated Body Fluid and Cytocompatibility of the Glasses

Bone bonding ability is the primary advantage of bioactive glasses. It is evaluated by examining the ability to form CaP/apatite on its surface in a Simulated Body Fluid (SBF) of which ion concentrations nearly equal to those of human blood plasma. However, the concentration of Cl^- in blood plasma (103.0 mM) is lower than that in SBF (147.8 mM). The concentration of HCO_3^- in blood plasma (27.0 mM) is much higher than that in SBF (4.2 mM). Correlation of the ability apatite to deposit on different biomaterials in SBF with their *in vivo* bone bioactivities, and some successful projects of novel bioactive materials based on the CaP/HCA formation on their surface in SBF have been reported. Kokubo *et al.* and Hench *et al.* have independently confirmed the formation of apatite on the surface of 45S5 Bioglass® proven to bond to living bones through a calcium phosphate (CaP) layer *in vivo* and in SBF.[67]

It is reported that the residual glass phase of bioactive glass-ceramics causes apatite formation on the surface. The residual glass phase provided a negatively charged surface developed during its corrosion in the surrounding solution. The negatively charged surface attracts Ca^{2+} and these Ca^{2+} accumulate at the glass-solution interface creating a solution highly supersaturated suitable for CaP formation.[68] This fact explains why a more dense calcium phosphate layer was observed on the surface of glass discs with amorphous structure. Almost no calcium phosphate deposited on the surface of any glass discs after soaking in SBF for 1 day, which can be attributed to the small quantity of ions released, presented by ion release profiles. The same situation was evident with on the crystalline samples after 7 days. However, obvious deposited calcium phosphate was observed on the surface of amorphous samples especially on the surface of amorphous *Ly-N* due to higher amount of ion release.

The SEM images of *Ly-N*, *Ly-C* and *Ly-S* with amorphous structure in SBF after 30 days are shown in Figure26. Much denser CaP layers formed on the surface of *Ly-N* and *Ly-C* but limited deposited CaP was observed on the surface of amorphous *Ly-S*. The images of energy dispersive X-ray (EDS) was used to prove the existence of CaP (the detail quantities of elements are shown in Figure 3 and Figure 4 in Appendix). According to the results of ion release profile, the concentration of Na^+ coming from amorphous *Ly-N* (216 μg/mL) is much higher than that of Sr^{2+} coming from amorphous *Ly-C* (9 μg/mL) and *Ly-S* (65 μg/mL) after 30 days, even though Na^+ and Sr^{2+} are both glass network modifiers. This fact explains why reduced CaP formed on the

surface of Sr-containing samples. This phenomenon also can be attributed to different atomic radius and charges of Na^{+} and Sr^{2+}.

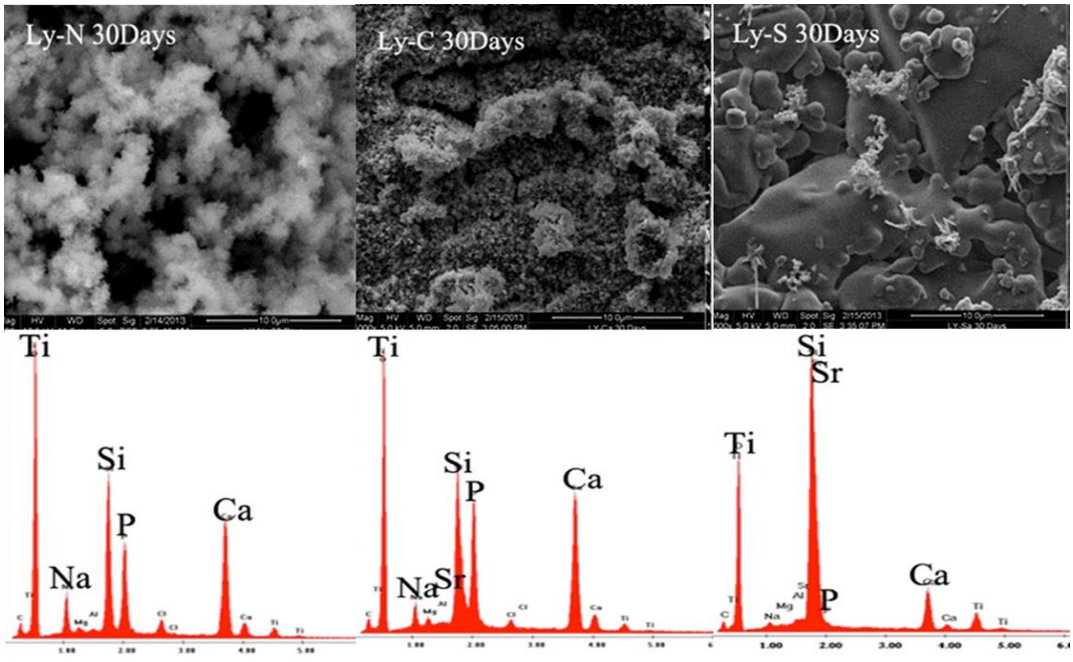

Figure 26. The SEM images and EDX of *Ly-N*, *Ly-C* and *Ly-S* with amorphous structure in SBF after 30 days.

High resolution SEM and XRD were conducted on *Ly-N* with amorphous structure coated with gold to determine whether the deposited layers on its surface is still amorphous CaP or has begun to turn into crystalline hydroxyapatite. The flake-like structure of the deposited layer presents an XRD pattern that after soaking in SBF for 30 days the surface of this layer began to crystallize. This crystalline structure is evident indicated by the new peaks appearing on the corresponding XRD pattern of the sample after SBF testing compared to that of the original sample (Figure 27). These peaks have been proven to be hydroxyapatite using *High Score Analysis*. There is a reasonable hypothesis: the deposited layers would turn into crystalline hydroxyapatite if it was soaked in SBF for more than 30 days.

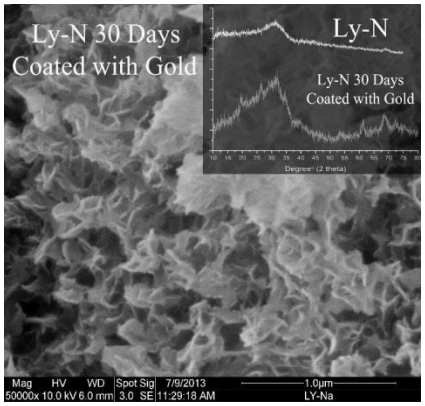

Figure 27. The SEM images Gold-coated *Ly-N* with amorphous structure in SBF for 30days and the XRD patterns of *Ly-N* with amorphous of structure before and after in SBF.

It has been reported in the literature that the crystallization of bioactive glasses would turn a bioactive glass into an inert material[69] due to the long-range orded structure, which reduce ion release rates, which coincides with the results of ICP testing. Therefore, limited formation of CaP was expected to deposit on the surfaces of the crystalline samples like the SEM images of *Ly-C* and *Ly-S* shown in Figure 28. However, *Ly-N* with crystalline structure was an exception was it was completely covered by the CaP deposited layers. There were two facts to explain the phenomena. The first was that HCA formation on the surfaces of controlled crystallized materials produced single crystal phase glass-ceramics and was proven to be bioactive. The crystal phase was identified as $1Na_2O{\cdot}2CaO{\cdot}3SiO$,[70] in other word, the pure $Na_2Ca_2SiO_3O_9$ phase which was the major crystal phase of *Ly-N*. The second explanation was a theory related to glass stability. Low values of Tc_1-T_g (Tc_1 is the onset crystallization temperature of glass, T_g is glass transit temperature) suggested a rapid tendency to crystallize for 45S5 Bioglass®.[59] In the terms of Tc_1-T_g values of the series glass , Tc_1-T_g values of *Ly-C* (128°C) and *Ly-S* (111°C) were lower than that of *Ly-N* (186°C), which indicates that *Ly-C* and *Ly-S* had greater tendency to form crystalline than *Ly-N* under the same heating rate (25°C/min). Therefore, it is reasonable to deduce that *Ly-C* and *Ly-S* had a greater crystalline fraction than *Ly-N* when they were sintered to reach T_{c1} leading to reduced ionic dissolution products ionic releasing productions and reduced formation of CaP.

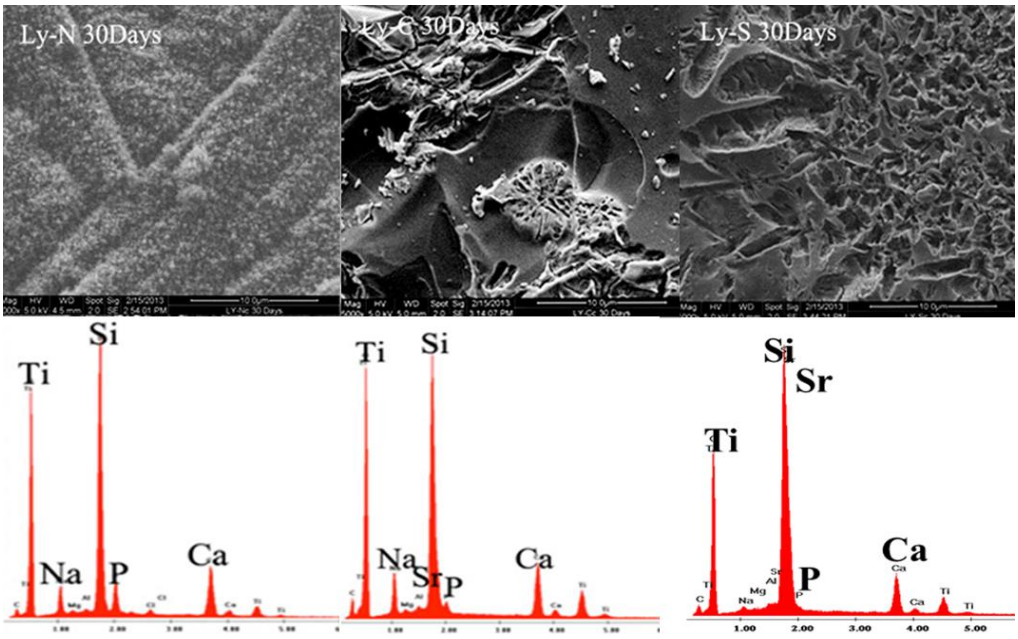

Figure 28. The SEM images and EDX of *Ly-N*, *Ly-C* and *Ly-S* with crystalline structure in SBF after 30 days.

Cell culture, in which L-929 fibroblast cells were used, was performed using the extracts of glass discs soaking in de-ionized water for 1, 7 and 30 days and the results are shown on Figure 29. Compared to the control group (sterile de-ions water instead of extracts), there was no significant decrease in the viability of cells with each glass extract with amorphous structure (p=0.006-1). However, there was significant decrease with *Ly-C* (p=0.001), *Ly-S* (p=0.000) after 1 day and *Ly-S* (p=0.000) after 7 days. However, the remaining amorphous material represented insignificant different levels of cell viability (p=0.027-0.028) after 7 days. There was no significant difference in the cell viability with each glass with a crystalline structure compared to the control group (p=0.024-1.000) except with *Ly-C* (p=0.000) after 7 days and *Ly-N* (p=0.002) after 30 days. However, no significant change existed in the cell viability among *Ly-N*, *Ly-C* and *Ly-S* with crystalline structure (p=0.028-1.000). According to these facts, the levels of ions leached from the series of glasses, both amorphous and crystalline structure, were not toxic to cells. In other words, the series of glasses were biocompatible.

It is obvious that *Ly-N* with amorphous structure increase the cell viability after 7 days and 30 days. The addition of Na^+ might explain this fact. A previous study has shown that, Na-containing bioactive glass (45S5 Bioglass® (in weight %): 45% SiO_2, 24.5% Na_2O, 24.5% CaO

and 6% P_2O_5) have better performance in the cell viability using fibroblast cells than other two no Na-containing bioactive glasses (55S: 60% SiO2, 36% CaO and 4% P_2O_5, and 77S: 80% SiO_2, 16% CaO and 4% P_2O_5).[71] However, the result refuses to support the results of cell viability testing in section 2: Sr-containing samples increased the cell viability. The positive influence of Sr^{2+} on the osteoblast cells can explain the phenomena. Previous study on a bioactive glass (containing 46.46 SiO_2 – 1.07 P_2O_5 – 26.38 Na_2O – 23.08 (SrO:CaO) where either no calcium (0%) or 10, 50 or 100% of the Ca^{2+} was substituted with Sr^{2+}) reported that significantly higher (osteoblast) cell viability activity of 100% Sr-substituted sample (SiO_2–P_2O_5–Na_2O–CaO) than that in any other group. [56]

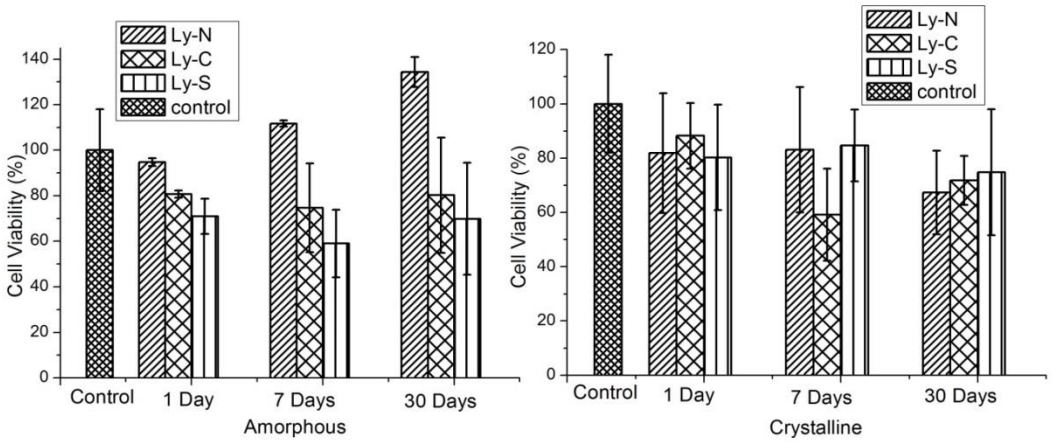

Figure 29. Cell Culture from sintered glass discs (amorphous/ crystalline) extracts in 1, 7 and 30 days.

Section Summary

This section determined that the Na^+ containing glasses and glass-ceramics consistently produced CaP surface layers more effectively than the Sr^{2+} containing materials, however, different morphology of CaP was observed with differences in glass composition. In addition, the CaP surface layer presented on *Ly-N* and *Ly- C* was observed to crystallize after 30 days. Cell culture conducted on the liquid extracts was observed to significantly increase cell viability in the Na^+ containing glasses, while no significant toxicity was experienced with the Sr^{2+} and crystalline analogues of each material. This study concludes that the inclusion of Na^+ significantly enhances the surface reactivity of bioactive glass/glass-ceramics, and that the addition of ions with different

electronic states can significantly influence the rate, atomic arrangement and morphology of the precipitated surface layer, and the associated cellular response.

CONCLUSION

Na^+ and Sr^{2+} are confirmed to be network modifiers, and each glass has a similar network structure and BO/NBO distribution. They also have very similar NC value. These facts indicate

that Na^+ and Sr^{2+} have almost the same influence on the structure of the series of bioactive glass. The results of cell viability presents that *Ly-N*, *Ly-C* and *Ly-S* do not have a negative influence on the viability and proliferation of these osteoblast cells. After soaking in the medium for 24h, the extract of *Ly-C* and *Ly*-S increase the proliferation of these cells. The extract of *Ly-C* for 48h has the same positive influence on the viability of the osteoblast cells. The SEM images of cell attachment presents that all the samples support the cell adhesion and spread, which indicates the biocompatibility and bioactivity of the glass series. More filopodia, flatter morphology and cell-cell contact of cells attached on the surface of Sr-containing (*Ly*-C and *Ly-S*) samples indicates that Sr^{2+} has better positive effect on the adhesion to bioactive glass surface than that of Na^+.

Glass powder discs with amorphous structure released more ions with a corresponding enhancement of pH values than the crystalline samples. The crystalline materials performed better mechanically in an aqueous environment with respect to time, while the amorphous material experienced significant reduction in hardness over time. These facts suggested that the crystalline structure can control the solubility and improve the mechanical durability of glass/glass-ceramic materials.

The Na^+ containing glass and glass-ceramics consistently produced CaP surface layers more effectively than the Sr^{2+} containing materials, however, different morphology of CaP was observed with differences in glass composition. In addition, the CaP surface layer on amorphous *Ly-N* and *Ly-C* was observed to crystallize after 30 days. Cell culture conducted on the liquid extracts was observed to significantly increase cell viability in the Na^+ containing glasses, while no significant toxicity was experienced with the Sr^{2+} and crystalline analogues of each material. This study concludes that the inclusion of Na^+ significantly enhances the surface reactivity of bioceramics, and that the addition of ions with different electronic states can significantly influence the rate, atomic arrangement and morphology of the precipitated surface layer, and the associated cellular response.

FUTURE WORK

The main objective of this project was to investigate the structure, solubility and bioactivity of the series of Na/Sr bioactive glasses, and to determine the influence of different compositions (Na/Sr) and structure (amorphous/crystalline) on the solubility and biocompatibility of bioactive

glasses/glass-ceramics. Based on the results of this work, the future studies of this glass series should include:

- Investigating biocompatibility, bioactivity, solubility and mechanical properties of scaffolds which are made of these glasses.
- Produce synthetic bone scaffolds which can be applied in clinical surgery is the final goal, however, animal testing will need to be conducted to determine the *in vivo* response and mechanical suitability.
- Cell culture testing (cell adhesion process) using osteoblast cells on the glasses/glass-ceramics with CaP/apatite surface layer already present to investigate whether osteoblast cells will preferentially attach and grow on these modified surfaces.
- Investigate the reason why the CaP layers formed on surface of different samples have different morphologies.

APPENDIX

Table I. Quantification from XPS High Resolution Spectra in Mole Fraction Including O and C

	Name	Position	FWHM	R.S.F.	Area	% Conc.
1899	Na 1s	1070.6	1.8	8.52	83488	17.0
LY-N	O 1s	529.8	3.0	2.93	90426	53.5
	Ti 2p	458.2	1.4	7.81	5813	1.3
	Ca 2p	346.4	1.5	5.07	23741	8.1
	C 1s	284.8	1.0	1	599	1.0
	Si 2p	101.5	1.8	0.817	8963	19.0
	O 1s_1	529.7	1.5	2.93	50091	29.5
	O 1s_2	531.3	1.5	2.93	40748	24.0
1900	O 1s	530.2	3.1	2.93	96763	61.3
LY-S	Ti 2p	458.6	1.5	7.81	5911	1.4
	Ca 2p	346.9	1.7	5.07	23554	8.6
	C 1s	284.8	0.8	1	400	0.7
	Si 2p	102.1	1.9	0.817	9087	20.6
	Sr 3d	133.5	3.1	5.05	19774	7.3
	O 1s_1	530.1	1.6	2.93	51771	32.8
	O 1s_2	531.8	1.7	2.93	45052	28.5
1901	Na 1s	1071.2	1.9	8.52	41482	10.0
LY-C	O 1s	529.9	3.0	2.93	81146	56.7
	Ti 2p	458.4	1.4	7.81	5214	1.4
	Ca 2p	346.6	1.6	5.07	20829	8.4
	C 1s	284.8	1.4	1	506	1.0
	Si 2p	101.8	1.9	0.817	7634	19.1
	Sr 3d	133.2	3.0	5.05	8287	3.4
	O 1s_1	529.9	1.5	2.93	44329	30.8
	O 1s	531.6	1.6	2.93	37179	25.9

Table II. Crystal Phases Identified for Ly-N, Ly-C and Ly-S

	Phase ID	Reference code	Crystal size (Å)
Ly-N	Combeite — $Na_{2.2}Ca_{1.9}Si_3O_9$	(Ref: 04-04-2757)	612
	Sodium — $Na_2Ca_3Si_6O_{16}$	(Ref: 04-012-8681)	591
Ly-C	Combeite — $Na_{4.8}Ca_3Si_6O_{18}$	(Ref: 04-007-5453)	N1000
	Silicon dioxide — SiO_2	(Ref: 04-007-5453)	N1000
Ly-S	Strontium silicon — Sr_2Si_3	(Ref: 01-089-2593)	348
	Titanium oxide — Ti_8O_{15}	(Ref: 04-007-0444)	138
	Calcium silicon — $CaSi_2$	(Ref: 04-007-0647)	229
	Strontium silicide — SrSi	(Ref: 01-076-7303)	317
	Strontium titanium silicate — $Sr_2TiSi_2O_8$	(Ref: 04-006-7366)	261
	Silicon oxide — SiO_2	(Ref: 00-029-0085)	N1000
	Perovskite — $CaTiO_3$	(Ref: 04-015-4851)	229

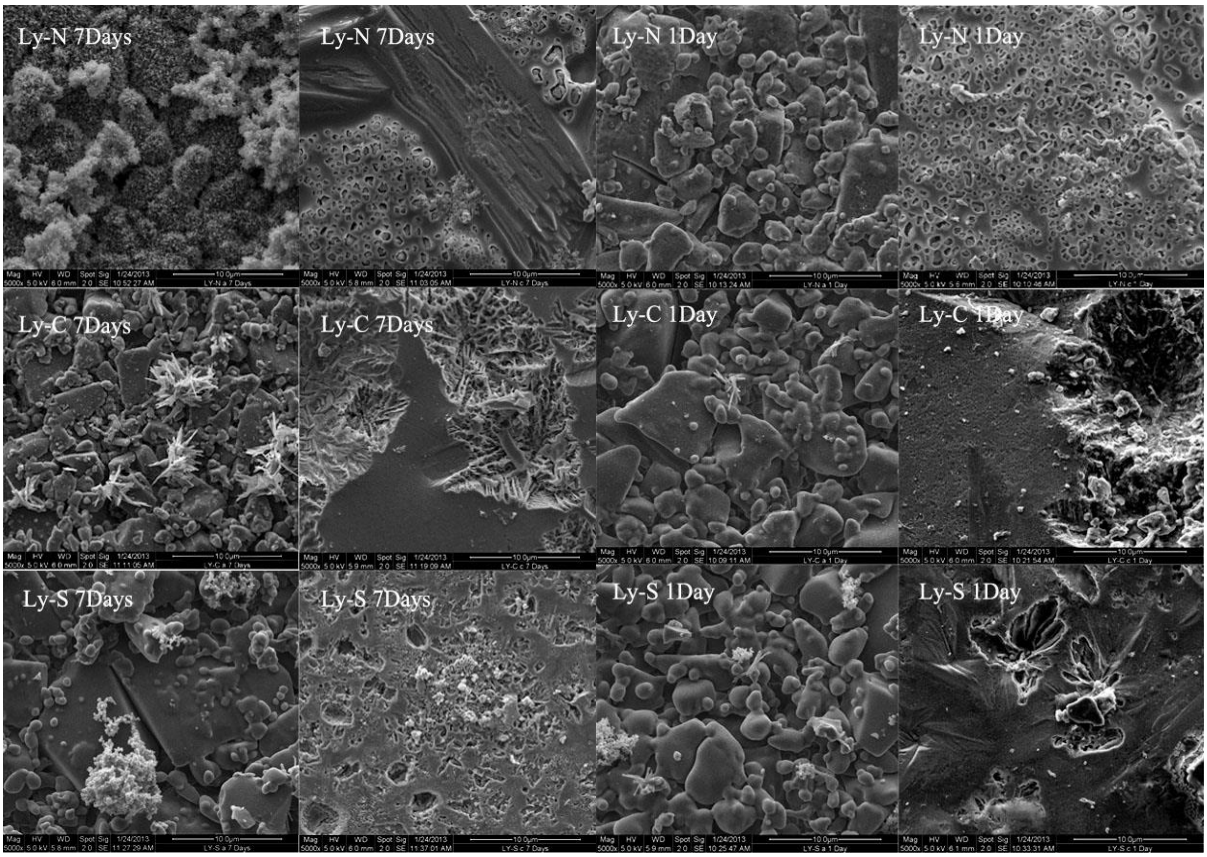

(a) (b) (c) (d)

Figure 1. SEM images of *Ly-N*, *Ly-C* and *Ly-S* after SBF 1 day with (a) amorphous (b) crystalline structure, and 7 days with (c) amorphous (d) crystalline structure.

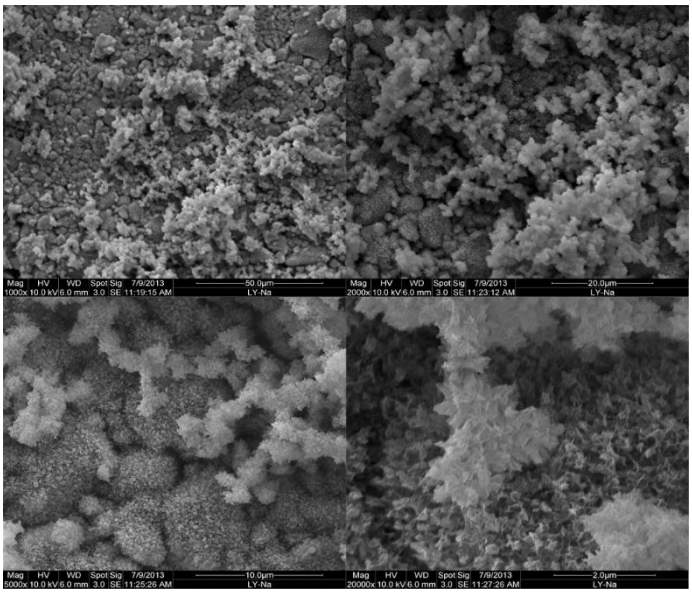

(a)

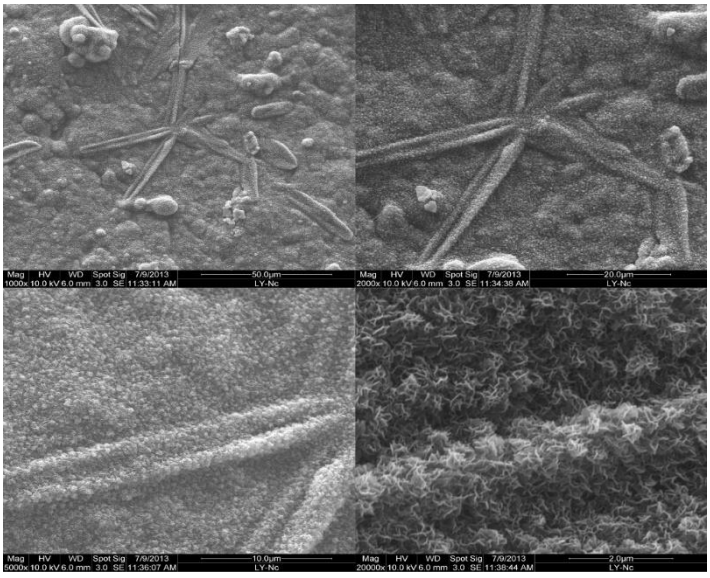

(b)

Figure 2. SEM images of *Ly-N* coated by gold with (a) amorphous (b) crystalline structure in SBF for 30 days.

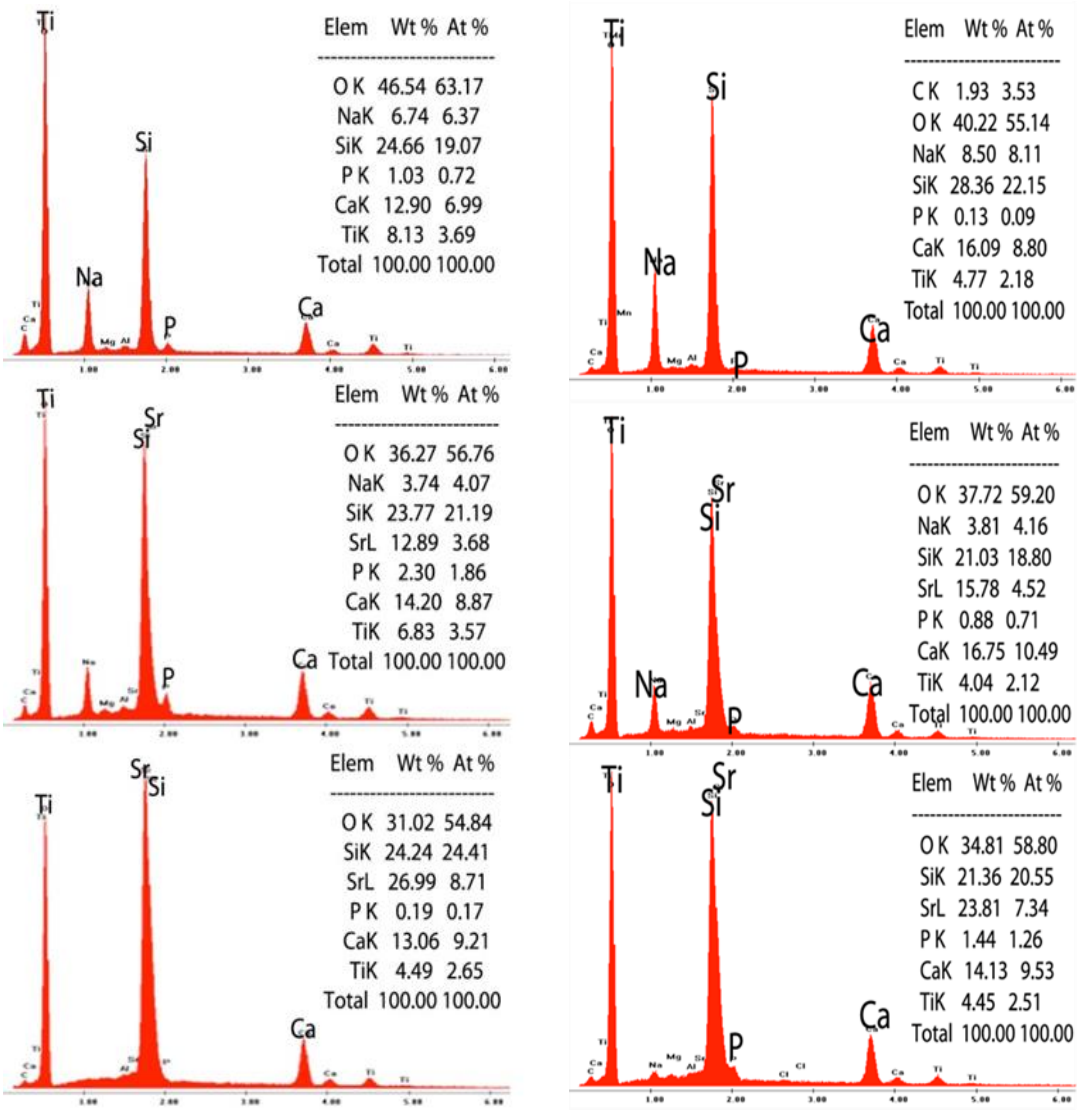

(a) (b)

Figure 3. Images of EDS and quantities of each element for *Ly-N*, *Ly-C* and *Ly-S* with (a) amorphous (b) crystalline structure in SBF for 1 days.

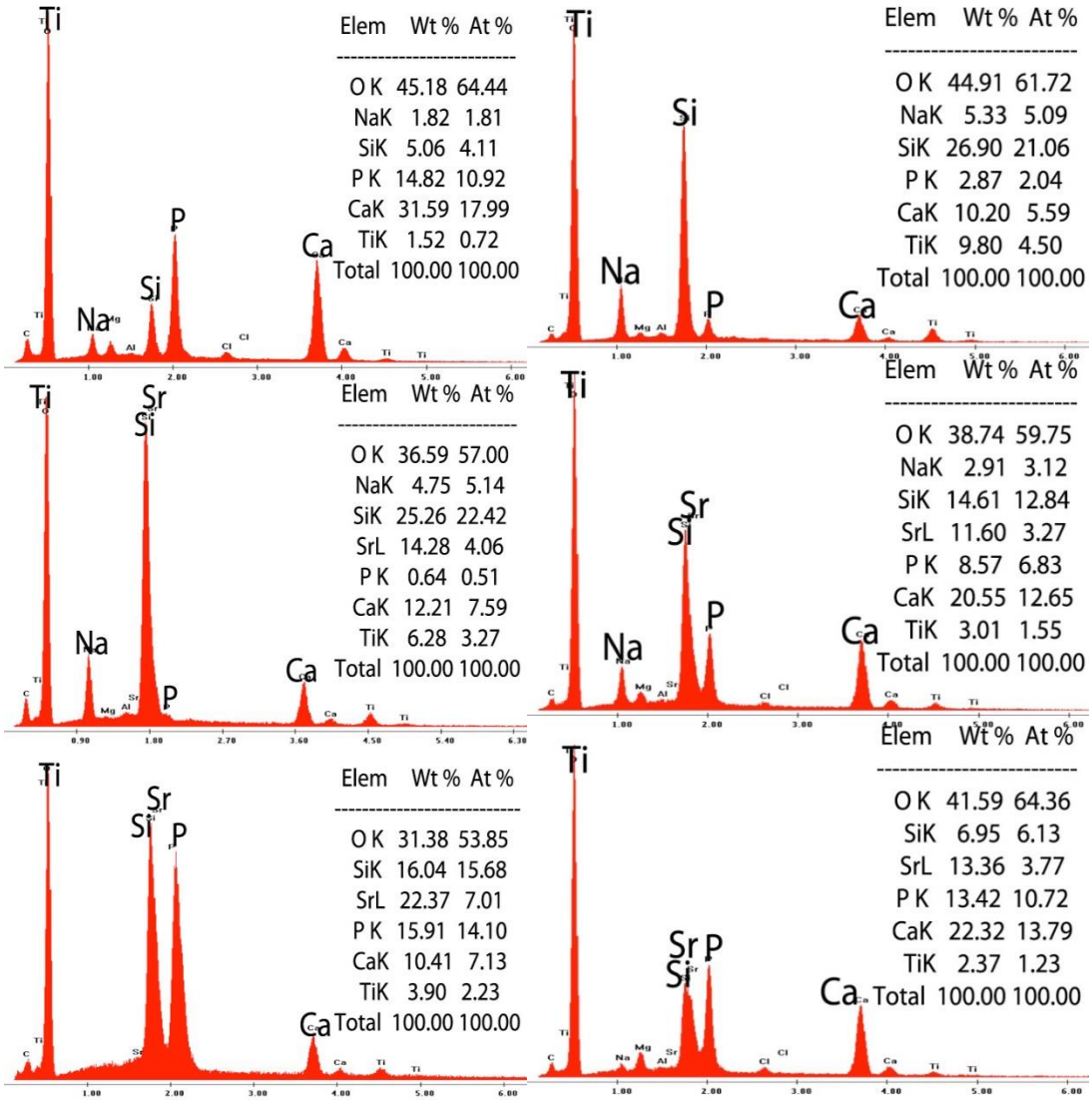

(a) (b)

Figure 4. Images of EDS and quantities of each element for *Ly-N*, *Ly-C* and *Ly-S* with (a) amorphous (b) crystalline structure in SBF for 7 days.

REFERENCES

1. J. M. P. L.L Hench, "Third-Generation Biomedical Materials," *Science,* **295** 1014-7 (2002).

2. L. L. Hench, "The Story of Bioglass®," *J. Mater. Sci. - Mater. Med.,* **17** 967-78 (2006).

3. J. E. Shelby, *Introduction to Glass Science and Technology,2nd Ed.;* pp. 3-5. The Royal Society of Chemistry, Cambridge, UK, 2005.

4. A. N. Cormack, "The Structure of Bioactive Glasses and Their Surfaces"; in *Bio-Glasses: An Introduction, the First Edition.* Edited by J. R. J. a. A. G. Clare. John Wiley & Sons, Ltd, 2012.

5. M. D. O'DonnelM., "Melt-Derived Bioactive Glass"; in *Bio-Glasses: An Introduction, the First Edition* Edited by J. R. J. a. A. G. Clare. John Wiley & Sons, Ltd, 2012.

6. S. Fujibayashi, M. Neo, H.-M. Kim, T. Kokubo, and T. Nakamura, "A Comparative Study between in Vivo Bone Ingrowth and in Vitro Apatite Formation on Na_2o–Cao–Sio_2 Glasses," *Biomaterials.,* **24** [8] 1349-56 (2003).

7. A. Tilocca and A. N. Cormack, "Surface Signatures of Bioactivity: Md Simulations of 45s and 65s Silicate Glasses," *Langmuir.,* **26** [1] 545-51 (2009).

8. H. Aguiar, J. Serra, P. González, and B. León, "Structural Study of Sol–Gel Silicate Glasses by Ir and Raman Spectroscopies," *J. Non-cryst. Solids.,* **355** [8] 475-80 (2009).

9. L. L. H. a. A. E. Clark., *Biocompatibility of Orthopaedic Implants, Vol.Ii* Edited by D. F. W. a. G. D. Winter. CRC Press, Boca Raton, Florida, 1982.

10. D. E. D. L. L. Hench, W. Höland, V. M. Rheinberger. , "Glass and Medicine," *Int. J. Appl. Glass. Sci,* **1** [1] 104-17 (2010).

11. J. R. Jones, "Review of Bioactive Glass: From Hench to Hybrids," *Acta Biomater.,* **9** 4457–86 (2013).

12. N. O. D.M. Reffitt, R .Jugdaohsingh, H.F.J. Cheung, B.A.J. Evans, R.P.H. Thompson, et al, "Orthosilicic Acid Stimulates Collagen Type 1 Synthesis and Osteoblastic Differentiation in Human Osteoblast-Like Cells in Vitro.," *Bone,* [32] 127–35 (2003).

13. L. L. Hench, "Genetic Design of Bioactive Glass," *J. Eur. Ceram. Soc.,* **29** [7] 1257-65 (2009).

14. A. J. E. I.D. Xynos, L.D. Buttery, L.L. Hench, J.M. Polak, " Ionic Products of Bioactive Glass Dissolution Increase Proliferation of Human Osteoblasts and Induce Insulin-Like Growth Factor Ii Mrna Expression and Protein Synthesis," *Biochem. Bioph. Res. Co,* **276** [2] 461-5 (2000).

15. M. D. J. Sandy, "Signal Pathways That Transduce Growth Factor-Stimulated Mitogenesis in Bone Cells," *Bone,* **23** [1] 17-26 (1998).

16. J. C. J. S. Mohan, T.A. Linkhart , D. J. Baylink, "Primary Structure of Human Skeletal Growth Factor: Homology with Human Insulin-Like Growth Factor-Ii.," *Biochim. Biophys. Acta, Gen. Subj.,* **966** [1] 44-55 (1988).

17. F. R. L. A.W. Wren, A. Kidari , M.R. Towler. .357 (2011) 1021–1026. , "The Structural Role of Titanium in Ca–Sr–Zn–Si/Ti Glasses for Medical Applications," *J. Non-Cryst. Solids,* **357** 10214-1026 (2011).

18. S. P. Nielsen, "The Biological Role of Strontium," *Bone,* **35** 583-8 (2004).

19. P. J. Marie, "Strontium Ranelate: New Insights into Its Dual Mode of Action," *Bone,* **40** [5] S5-S8 (2007).

20. Y. Jiang, H. Genant, and J. Zhao, "Effect of Strontium Ranelate on 3d Cortical and Trabecular Microstructure in Postmenopausal Osteoporosis in Multicenter, Double-Blind, and Placebo Controlled Studies," *J. Bone. Miner. Res.,* **21** 44 (2006).

21. A. A. Gorustovich, T. Steimetz, R. L. Cabrini, and J. M. Porto López, "Osteoconductivity of Strontium ‐ Doped Bioactive Glass Particles: A Histomorphometric Study in Rats," *J. Biomed. Mater. Res. Part A,* **92** [1] 232-7 (2010).

22. A. Doublier, D. Farlay, M. T. Khebbab, X. Jaurand, P. J. Meunier, and G. Boivin, "Distribution of Strontium and Mineralization in Iliac Bone Biopsies from Osteoporotic Women Treated Long-Term with Strontium Ranelate," *Eur. J. Endocrinol.,* **165** [3] 469-76 (2011).

23. P. L. C. M.D. O'Donell, C.A. Miller, E. Gentleman and M.M. Stevens, "Materials Characterization and Cytotoxic Assessment of Strontium-Substituted Bioactive Glasses for Bone Regeneration.," *J. Mater. Chem.,* **10** 8934-41 (2010).

24. S. Dahl, P. Allain, P. Marie, Y. Mauras, G. Boivin, P. Ammann, Y. Tsouderos, P. Delmas, and C. Christiansen, "Incorporation and Distribution of Strontium in Bone," *Bone,* **28** [4] 446-53 (2001).

25. R. G. H. M.D. O'Donnell, "Influence of Strontium and the Importance of Glass Chemistry and Structure When Designing Bioactive Glasses for Bone Regeneration," *Acta Biomater.,* **6** 2382–5 (2010).

26. L. L. Hench, " Bioceramics," *J. Am. Ceram. Soc.,* **81** 1705-28 (1998).

27. E. Verne, " Bioactive Glass and Glass-Ceramic Coatings"; in *Bio-Glasses: An Introduction, the First Edition.* Edited by J. R. J. a. A. G. Clare. John Wiley & Sons, Ltd, 2012.

28. C. V. B. S. D. Nunzioa, S. Spriano, D. Milanese, E. Verne´, V. Bergo, G. Maina, P. Spinelli, "Silver Containing Bioactive Glasses Prepared by Molten Salt Ion-Exchange," *J. Eur. Ceram. Soc.,* **24** 2935–42 (2004).

29. E. S. S. Lopez-Estebana, S. Fujino, T. O ku, K. Suganuma, A.P. Tomsia, "Bioactive Glass Coatings for Orthopedic Metallic Implants," *J. Eur. Ceram. Soc.,* **23** 2921–30 (2003).

30. M. F. E. Verne, A. Ventrella, L. Paracchini, A. Krajewski and A. Ravaglioli, "Sintering and Plasma Spray Deposition of Bioactive Glass-Matrix Composites for Medical Applications," *J. Eur. Ceram. Soc.,* **18** 363-72 (1998).

31. M. B. E. Verne", C. Vitale Brovarone, C. Moisescuc, F. Lupo, S. SprianoM. Cannas, "Fluoroapatite Glass-Ceramic Coatings on Alumina: Structural, Mechanical and Biological Characterization," *Biomaterials.,* **23** 3395–403 (2002).

32. B. C. V. E .Verne, A. Ravaglioli, A. Krajewski, "Multilayered Bioactive Coatings on Al_2O_3 Substrates," *Bioceramics,* 491-4 (1999).

33. A. N. N. M. Fini, M.G. Gandolfi, et al, "Biomaterials for Orthopedic Surgery in Osteoporotic Bone: A Comparative Study in Osteopenic Rats," *International Journal of Artificial Organs,* **20** [5] 291-7 (1997).

34. M. O. K. Shimizu, P. Kumar, Y. Kotoura, T. Yamamuro, K. Makinouchi, T. Nakamura, "Time-Dependent Changes in the Mechanical Properties of Zirconia Ceramic.," *J. Biomed. Mater. Res. Part A,* **27** [6] 729-34 (1993).

35. V. Stanic, N. Nicoli Aldini, M. Fini, G. Giavaresi, R. Giardino, A. Krajewski, A. Ravaglioli, M. Mazzocchi, B. Dubini, and M. Ponzi Bossi, "Osteointegration of Bioactive Glass-Coated Zirconia in Healthy Bone: An in Vivo Evaluation," *Biomaterials.,* **23** [18] 3833-41 (2002).

36. E. Verne, M. Ferraris, A. Ventrella, L. Paracchini, A. Krajewski, and A. Ravaglioli, "Sintering and Plasma Spray Deposition of Bioactive Glass-Matrix Composites for Medical Applications," *J. Eur. Ceram. Soc.,* **18** [4] 363-72 (1998).

37. V. Stanica, N. N. Aldinic, M. Finic, G. Giavaresic et al, "Osteointegration of Bioactive Glass-Coated Zirconia in Healthy Bone: An in Vivo Evaluation," *Biomaterials.,* **23** 3833–41 (2002).

38. A. R. A. Krajewski, M. Mazzocch, M. Fini, "Coating of Zro_2 Supports with a Biological Glass. Journal of Materials Science," *J. Mater. Sci. - Mater. Med.,* **9** [6] 309-16 (1998).

39. E. S. Q.Fu , M.N. Rahaman, P.Antoni, Tomsia, "Bioactive Glass Scaffolds for Bone Tissue Engineering: State of the Art and Future Perspectives," *Mater. Sci. Eng., C,* **31** 1245–56 (2011).

40. A. M. S. Eqtesadi, P. Miranda, "Robocasting of 45s5 Bioactive Glassscaffoldsfor Bone Tissue Engineering," *J. Eur. Ceram. Soc.,* **34** 107-18 (2014).

41. M. N. R. M. A. Deliormanlı, "Direct-Write Assembly of Silicate and Borate Bioactive Glassscaffoldsfor Bone Repair " *J. Eur. Ceram. Soc.,* **32** 3637–46 (2012).

42. J. R. Jones., "Bioactive Glass as Synthetic Bone Grafts and Scaffolds for Tissue Engineering"; in *Bio-Glasses: An Introduction, the First Edition.* Edited by J. R. J. a. A. G. Clare. John Wiley & Sons, Ltd, 2012.

43. Q. Z. C. K. Rezwan, J.J. Blaker, A. R. Boccaccini, "Biodegradable and Bioactive Porous Polymer/Inorganic Composite Scaffolds for Bone Tissue Engineering," *Biomaterials.,* **27** 3413–31 (2006).

44. M. N. R. Q. Fu, B. S. Bal. M, "Echanical and in Vitro Performance of 13–93 Bioactive Glass Scaffolds Prepared by a Polymer Foam Replication Technique," *Acta Biomater.,* **4** 1854–64 (2008).

45. J. R. J. a. Q.-Z. C. A.R. Boccaccini, "Composites Containing Bioactive Glass"; in *Bio-Glasses: An Introduction, the First Edition.* Edited by J. R. J. a. A. G. Clare. John Wiley & Sons, Ltd, 2012.

46. J. Franco, P. Hunger, M. E. Launey, A. P. Tomsia, and E. Saiz, "Direct Write Assembly of Calcium Phosphate Scaffolds Using a Water-Based Hydrogel," *Acta Biomater.,* **6** [1] 218-28 (2010).

47. A. R. B. V. Maquet, L. Pravata, I. Notingher, R. Je´roˆme, "Preparation, Characterization, and in Vitro Degradation of Bioresorbable and Bioactive Composites Based on Bioglasss-Filled Polylactide Foams," *J. Biomed. Mater. Res. Part A,* **66A** 335–46 (2003).

48. C. L. R. M. W. Helena, J. J. Blakerb, J.E. Gough, "Three-Dimensional Culture of Annulus Fibrosus Cells within Pdlla/ Bioglass® Composite Foam Scaffolds: Assessment of Cell Attachment, Proliferation and Extracellular Matrix Production," *Biomaterials.,* **28** 2010–20 (2007).

49. N. Barroca, A. Daniel-da-Silva, P. Vilarinho, and M. Fernandes, "Tailoring the Morphology of High Molecular Weight Plla Scaffolds through Bioglass Addition," *Acta Biomater.,* **6** [9] 3611-20 (2010).

50. J. S. P. Gonzalez, S. Liste, S. Chiussi, B. Leon, M. Perez-Amor, "Raman Spectroscopic Study of Bioactive Silica Based Glasses," *J. Non-cryst. Solids.,* **320** 92-9 (2003).

51. I. E. Wachs, "Raman and Ir Studies of Surface Metal Oxide Species on Oxide Supports: Supported Metal Oxide Catalysts," *Catal. Today,* **27** [3] 437-55 (1996).

52. J. Serra, P. González, S. Liste, C. Serra, S. Chiussi, B. León, M. Pérez-Amor, H. Ylänen, and M. Hupa, "Ftir and Xps Studies of Bioactive Silica Based Glasses," *J. Non-cryst. Solids.,* **332** [1] 20-7 (2003).

53. I. Elgayar, A. Aliev, A. Boccaccini, and R. Hill, "Structural Analysis of Bioactive Glasses," *J. Non-cryst. Solids.,* **351** [2] 173-83 (2005).

54. E. Robert, A. Whittington, F. Fayon, M. Pichavant, and D. Massiot, "Structural Characterization of Water-Bearing Silicate and Aluminosilicate Glasses by High-Resolution Solid-State Nmr," *Chem. Geol.,* **174** [1] 291-305 (2001).

55. C. Loty, J. Sautier, M. Tan, M. Oboeuf, E. Jallot, H. Boulekbache, D. Greenspan, and N. Forest, "Bioactive Glass Stimulates in Vitro Osteoblast Differentiation and Creates a Favorable Template for Bone Tissue Formation," *J. Bone. Miner. Res.,* **16** [2] 231-9 (2001).

56. E. Gentleman, Y. C. Fredholm, G. Jell, N. Lotfibakhshaiesh, M. D. O'Donnell, R. G. Hill, and M. M. Stevens, "The Effects of Strontium-Substituted Bioactive Glasses on Osteoblasts and Osteoclasts *in Vitro*," *Biomaterials.,* **31** [14] 3949-56 (2010).

57. G. Passeri, A. Cacchioli, F. Ravanetti, C. Galli, E. Elezi, and G. M. Macaluso, "Adhesion Pattern and Growth of Primary Human Osteoblastic Cells on Five Commercially Available Titanium Surfaces," *Clin. Oral Implan. Res,* **21** [7] 756-65 (2010).

58. N. Olmo, A. I. Martín, A. J. Salinas, J. Turnay, M. a. Vallet-Regí, and M. A. Lizarbe, "Bioactive Sol–Gel Glasses with and without a Hydroxycarbonate Apatite Layer as Substrates for Osteoblast Cell Adhesion and Proliferation," *Biomaterials.,* **24** [20] 3383-93 (2003).

59. L. L. H. D.C. Clypper, "Crystallization Kinetics of Tape Cast Bioactive Glass 45s5.," *J. Non-cryst. Solids.,* **318** 43-8 (2003).

60. R. Ravarian, F. Moztarzadeh, M. S. Hashjin, S. Rabiee, P. Khoshakhlagh, and M. Tahriri, "Synthesis, Characterization and Bioactivity Investigation of Bioglass/Hydroxyapatite Composite," *Ceram. Int.,* **36** [1] 291-7 (2010).

61. D. Zhang, E. Vedel, L. Hupa, H. T. Aro, and M. Hupa, "Predicting Physical and Chemical Properties of Bioactive Glasses from Chemical Composition. Part 3: In Vitro Reactivity," *Glass Technol.: Eur. J. Glass Sci. Technol., Part A,* **50** [1] 1-8 (2009).

62. M. Grynpas, E. Hamilton, R. Cheung, Y. Tsouderos, P. Deloffre, M. Hott, and P. Marie, "Strontium Increases Vertebral Bone Volume in Rats at a Low Dose That Does Not Induce Detectable Mineralization Defect," *Bone,* **18** [3] 253-9 (1996).

63. S. Murphy, A. Wren, M. Towler, and D. Boyd, "The Effect of Ionic Dissolution Products of Ca–Sr–Na–Zn–Si Bioactive Glass on in Vitro Cytocompatibility," *J. Mater. Sci. - Mater. Med.,* **21** [10] 2827-34 (2010).

64. S. Kashyap, K. Griep, and J. A. Nychka, "Crystallization Kinetics, Mineralization and Crack Propagation in Partially Crystallized Bioactive Glass 45s5," *Mater. Sci. Eng., C,* **31** [4] 762-9 (2011).

65. S. Deb and J. Nicholson, "The Effect of Strontium Oxide in Glass–Ionomer Cements," *J. Mater. Sci. - Mater. Med.,* **10** [8] 471-4 (1999).

66. I. Farooq, Z. Imran, U. Farooq, A. Leghari, and H. Ali, "Bioactive Glass: A Material for the Future," *World Journal of Dentistry,* **3** [2] (2012).

67. H. T. T. Kokubo, "How Useful Is Sbf in Predicting in Vivo Bone Bioactivity?," *Biomaterials.,* **27** 2907-15 (2006).

68. P. Li, Q. Yang, F. Zhang, and T. Kokubo, "The Effect of Residual Glassy Phase in a Bioactive Glass-Ceramic on the Formation of Its Surface Apatite Layerin Vitro," *J. Mater. Sci. - Mater. Med.,* **3** [6] 452-6 (1992).

69. Q. Z. Chen, I. D. Thompson, and A. R. Boccaccini, "45s5 Bioglass®-Derived Glass–Ceramic Scaffolds for Bone Tissue Engineering," *Biomaterials.,* **27** [11] 2414-25 (2006).

70. O. Peitl, E. Dutra Zanotto, and L. L. Hench, "Highly Bioactive P2o5–Na2o–Cao–Sio2 Glass-Ceramics," *J. Non-cryst. Solids.,* **292** [1–3] 115-26 (2001).

71. I. A. Silver, J. Deas, and M. Erecińska, "Interactions of Bioactive Glasses with Osteoblasts in Vitro: Effects of 45s5 Bioglass®, and 58s and 77s Bioactive Glasses on Metabolism, Intracellular Ion Concentrations and Cell Viability," *Biomaterials.,* **22** [2] 175-85 (2001).